The Science and Technology Journal of AWE

Discovery 19

September 2009

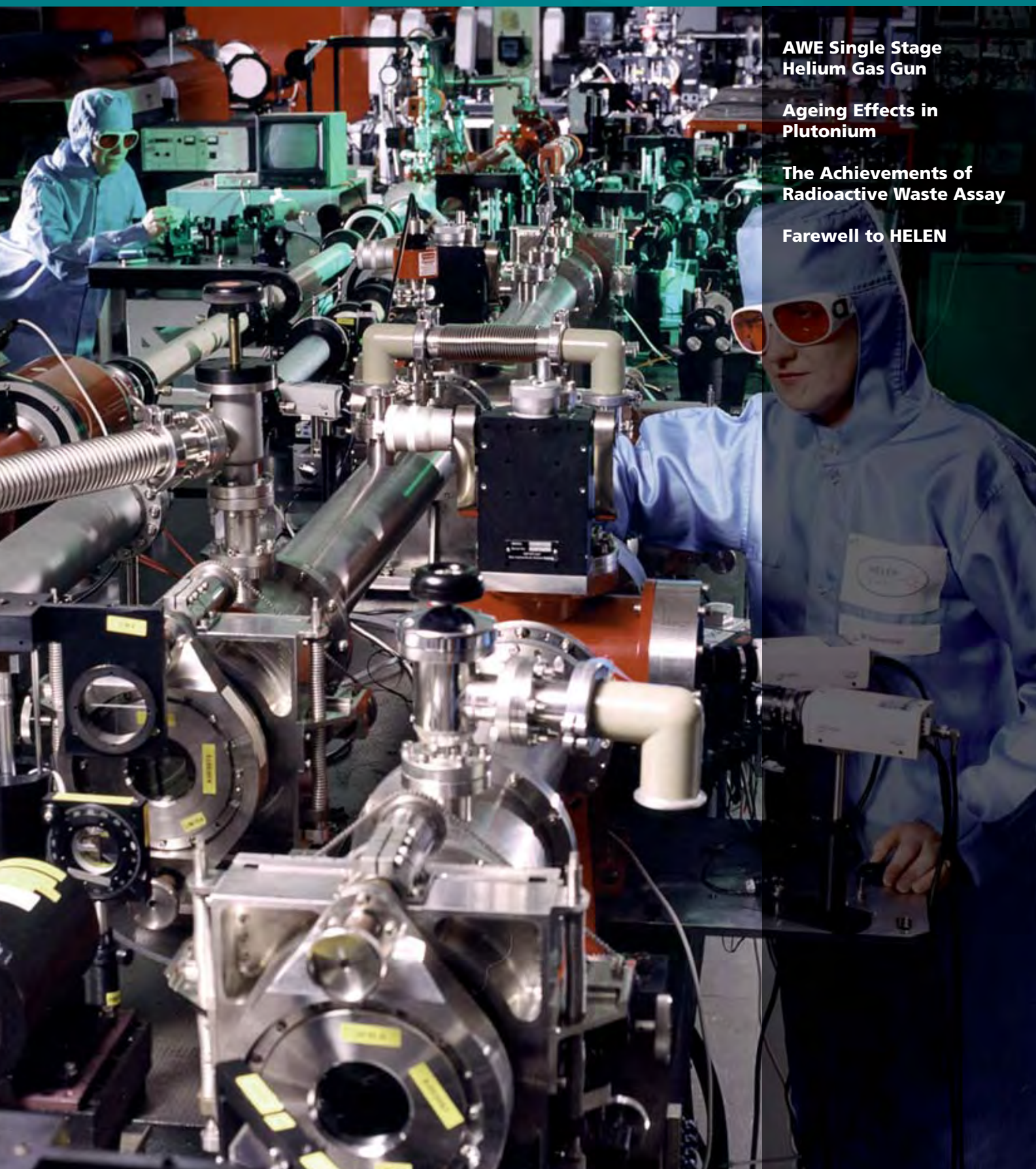

Discovery

Contents

cover image
Image of HELEN (High Energy Laser Embodying Neodymium). Commissioned in 1979

19

It is my pleasure to introduce this, the 19th edition of Discovery, a window into the wide range of science, engineering and technology at AWE. As Chief Executive Officer since May 2009 I have already been impressed with both the breadth and depth of activity at AWE and have come across many examples of high quality work in the physical sciences, engineering, materials and chemistry.

My visits and briefings within the Company have highlighted both theoretical and experimental studies with a marked and increasing emphasis on modelling and simulation.

These studies complement an expanding outreach programme including strategic alliances with a number of UK universities - in addition to strong collaborations with our colleagues in the US National Nuclear Laboratories at Los Alamos, Livermore and Sandia.

All this comes at a time when important decisions are being made by the Government to ensure the continuation of a UK nuclear deterrent into the future. The skyline at both Aldermaston and Burghfield sites will be changing rapidly as new investments in science, engineering, technology and manufacturing facilities come on stream or begin their journey through feasibility and design.

This edition continues to highlight the wide range of work at AWE. There is an article on helium gas guns to study fundamental properties of materials, a further update on the complex nature of ageing effects in plutonium, the development of radioactive material waste assaying and a final farewell to AWEs high power laser, HELEN.

In closing I hope you enjoy reading this latest edition of Discovery. AWE makes a vital contribution to strategic defence and this is underpinned by its science, engineering and technology capabilities. Many of these are at the forefront of science and technology – some are unique to the UK as we continue to improve our understanding of processes taking place under extreme conditions of pressure and temperature involving a wide range of both conventional and unusual metallic and non-metallic materials selected for their inherent properties.

It is truly an exciting period in AWEs long and distinguished history.

Mr Robin McGill
Chief Executive Officer

AWE Single Stage Helium Gas Gun

A major part of AWE's mission is to be able to underwrite the performance and safety of the UK deterrent without recourse to nuclear testing. The initial operation of a nuclear weapon involves materials being shock loaded with a detonating explosive. To accurately calculate performance and safety we require simple and accurate shock compression data to develop and validate the material models used with our modern hydrocodes and supercomputers.

This data can be generated with explosively driven experiments but the nature of a detonation wave leads to shock waves that attenuate in an inert material. This makes the task of developing accurate material models difficult as the hydrocode must accurately model the explosive drive as well as the material.

A convenient way to generate a sustained, constant pressure shock is by the plate impact technique. One flat plate is impacted flush onto another and an initially square shock pulse is generated in the target plate. The flyer plate is usually accelerated down a large (50 mm diameter or larger) smooth bored gun, driven by either a chemical propellant (gunpowder) or compressed gas, onto a stationary target plate that is precisely aligned with the barrel of the gun. The velocity of the flyer plate can be controlled by the propellant fill or gas pressure and the projectile mass, allowing a systematic study of material response to varying shock stress. This allows the study of effects such as shock driven phase transformations and tensile or spall failure strengths.

Access to both loading techniques is desirable for a healthy hydrodynamics capability. AWE has always operated several firing chambers for explosives trials. In 2002 a programme was started to reinstate a plate impact capability at AWE. This article explains the work of this programme and the creation of the AWE plate impact helium gas gun.

Single and Two Stage Gas Guns

A schematic of a single stage gas driven gun is shown in Figure 1. A high pressure reservoir is filled with the drive gas to the required firing pressure. This high pressure volume is then connected to the evacuated barrel containing the projectile by the operation of a fast acting gas valve or bursting diaphragm arrangement. The projectile is accelerated down the barrel by the high pressure gas which reduces the driving pressure as the gas expands down the barrel.

The acceleration of the projectile is not smooth as a

FIGURE 1

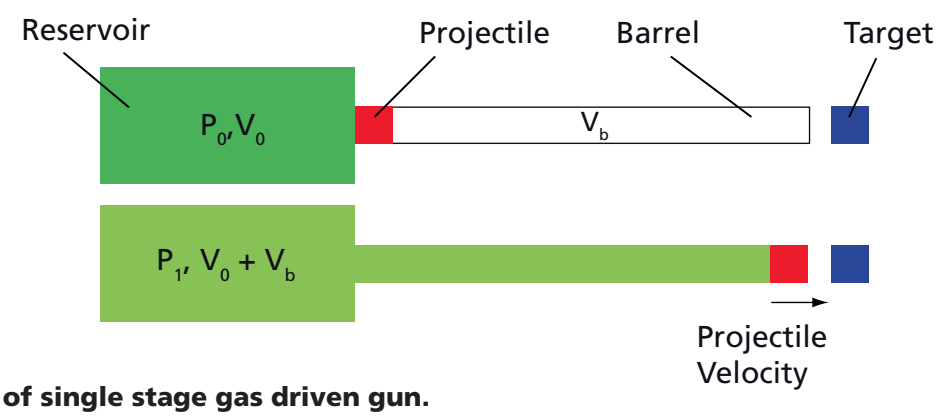

Schematic of single stage gas driven gun.

series of release waves are initiated by the valve opening which reverberate in the barrel and reservoir increasing the projectile velocity in steps. The final projectile velocity is controlled by the initial reservoir pressure and the sabot mass. The complex wave reverberations can be approximated to a reasonable degree of accuracy by a simple treatment of the first rarefaction wave in the gas. This gives the projectile velocity (u) as:

$$u = \frac{2C_0}{\gamma - 1}\left[1 - \left(\frac{P}{P_0}\right)^{\frac{\gamma - 1}{2\gamma}}\right] \quad (1)$$

Where P is the instantaneous pressure, P_0 is the initial pressure and where γ is the ratio of specific heat of constant pressure and volume (C_p/C_v) The key drive gas properties for gun performance are the sound speed (C_0) and γ. At low pressures the velocity is determined mainly by the value $C_0/(\gamma\text{-}1)$. Table 1 shows these values for commonly used drive gases.

TABLE 1

Gas	C_0 (ms^{-1})	γ (C_p/C_v)	$C_0/(\gamma\text{-}1)$
Hydrogen	1238	1.41	3019
Helium	966	1.63	1533
Air	330	1.4	825
Argon	307	1.67	458

Gas performances for single stage gas guns.

The operation of a two stage gas gun is shown schematically in Figure 2. A large bore first stage gas gun known as the pump tube is used to dynamically create a higher pressure reservoir of gas to drive the projectile in the smaller bore second stage. The pump tube is filled with a drive gas to a low pressure. A gas or powder drive is used to fire the pump tube piston (usually polyethylene) to compress the low pressure gas in the pump tube. As the piston approaches the transition section, where the diameter of the tube decreases, a very high pressure gas region is created which is the reservoir for the second stage. This high pressure ruptures a bursting diaphragm behind the projectile which then accelerates, in a similar way to a single stage gun. The polyethylene piston impacts the conical transition section,

FIGURE 2

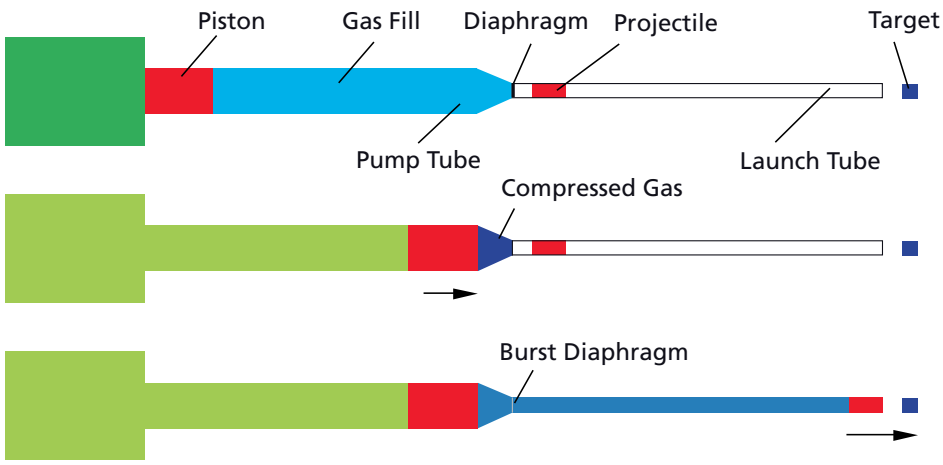

Schematic of two stage gas gun.

FIGURE 3

AWE helium driven gas gun.

TABLE 2

Gun Type	Gas Driven (Kms^{-1})	Powder Driven (Kms^{-1})
Single Stage Gun	0 - 1.4	0.5 - 2.5
Two Stage Gun	1.5 - 4.0	2.0 - 5.5

Projectile velocities of different guns.

typically extruding into this space, sealing the pump tube from the second stage.

Table 2 shows typical performance regimes for large bore (>50 mm) single and two stage gas and powder driven guns.

AWE Single Stage He Gas Gun

The AWE gas gun is a single stage helium (He) driven gas gun with a fast acting gas valve and a distributed reservoir as shown in Figure 3. He was chosen for the primary driver due to its chemical inertness although it delivers marginally lower performance than hydrogen over the usual pressure ranges. The barrel is 3 m long and the smooth bore is 70 mm in diameter.

The AWE gas gun is capable of firing projectiles weighing 200 g at velocities up to 900 ms^{-1} at maximum firing pressure. This equates to the same kinetic energy as a small car travelling at 30 mph. The high pressure He gas reservoirs are the six cylinders arranged around the main barrel and have a total volume of 13 litres. At the maximum fill pressure of 272 bar (4,000 psi) the reservoirs hold 3500 litres of He at normal atmospheric pressure. To operate the AWE gas gun a polycarbonate cylinder (referred to as the sabot) with the flyer plate attached to the front is loaded into the barrel and the breech is bolted into place, as shown in Figure 4a. Some He is then passed from the He supply bottles into the trigger chamber behind the aluminium (Al) piston valve as shown in Figure 4b. This forces the valve closed, sealing the reservoirs from the barrel.

The reservoirs and trigger chamber are then charged together to the desired firing pressure. The larger area of the trigger chamber face of the valve, compared to the small conical section, ensures the valve remains sealed. The barrel and target chamber are evacuated to around 10 mbar to prevent a column of air

FIGURE 4a

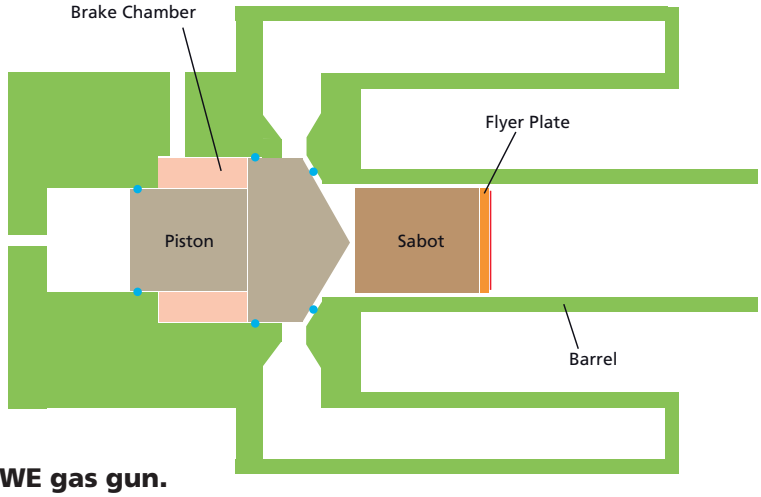

Loading stage of AWE gas gun.

FIGURE 4b

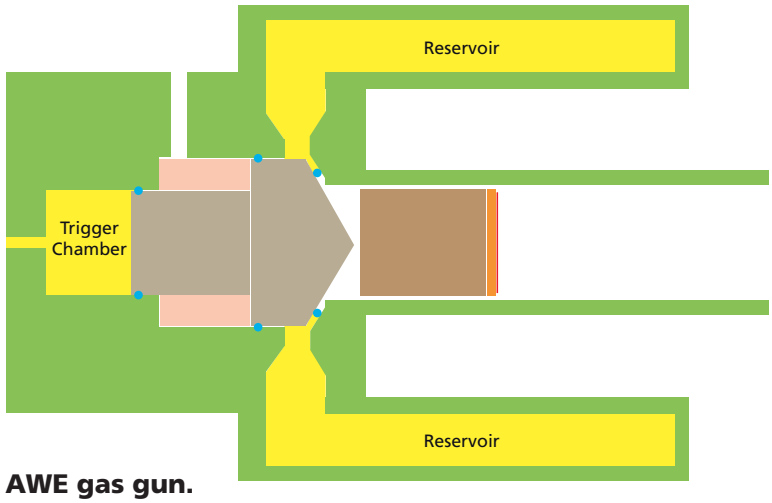

Pre-firing stage of AWE gas gun.

FIGURE 4c

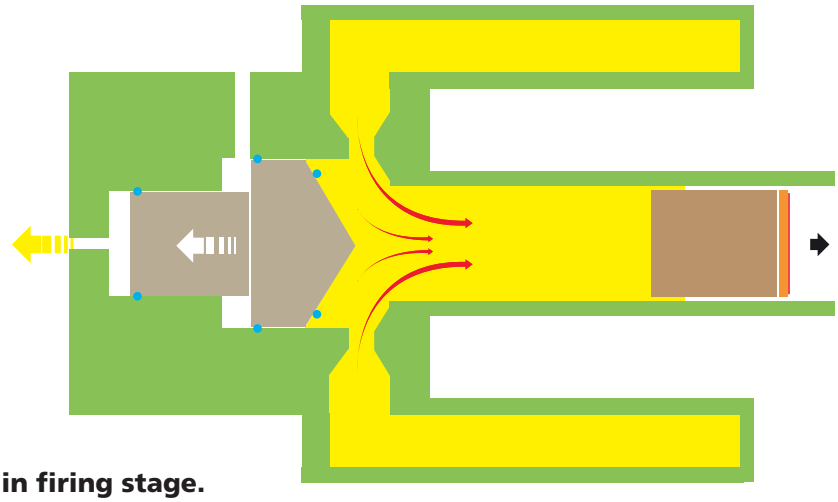

AWE gas gun in firing stage.

being pushed down the barrel ahead of the flyer. To fire the gun the trigger chamber is vented and the valve opens when the force from the reservoir gas exceeds the force from the trigger chamber. The reservoir gas then flows behind the sabot, opening the valve more rapidly and accelerating the sabot and flyer plate down the barrel, as shown in Figure 4c.

The design of the AWE gas gun breech originated in the hydrodynamics department in the 1970s.[1] The design incorporates a brake chamber volume that is separate from the high pressure system. This chamber can be filled with compressed air to a few bar or evacuated with a vacuum pump. This allows the valve to be decelerated before impacting the rear of the breech for high pressure shots and improves the reproducibility of firing at low pressures respectively.

A typical plate impact experimental arrangement is shown in Figure 5. An Al vacuum vessel is sealed to the end of the barrel around the target with a thin mylar or perspex bursting disc behind the target. This is designed to allow the target and sabot to exit the target chamber into the catch tank after impact. The target is held in a mounting ring which is aligned to the barrel with precisely machined support collars. This ensures that the flyer plate attached to the sabot will impact the target plate with less than 0.001 rad (0.057°) tilt between them. This is the required accuracy to generate one-dimensional strain conditions in the sample. The sample is attached to the mounting ring with sacrificial washers or solder tabs which fail when the target plate is impacted allowing the target and sabot to exit the vacuum chamber through the bursting disc.

FIGURE 5

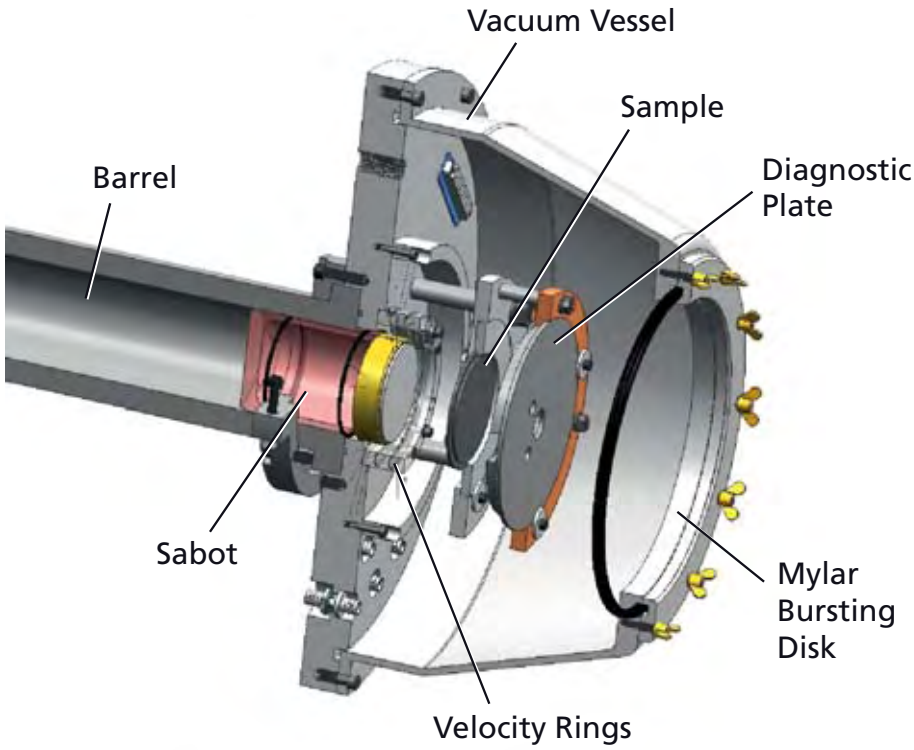

Three dimensional model of the AWE Gas Gun target chamber.

FIGURE 6

Diagnostic equipment and catch tank for AWE gas gun.

The gun and gas systems are housed in an annexe room adjacent to the firing chamber which houses the target end of the barrel. The catch tank and the diagnostic equipment are shown in Figure 6. The catch tank used for the AWE gas gun is a thick walled 3 foot diameter steel vessel weighing approximately 1000 kg. Several steel plates are hung from the top port of the vessel, which is also filled with rags, to catch the sample and projectile debris emerging from the vacuum chamber. Typical recovered debris from a plate impact trial is shown in Figure 7.

Data Collection

To determine the material states and effects created by the shock loading process a range of high speed diagnostics is employed on the gas gun. On every shot a projectile velocity measurement is made using two rings of electrical contact pins mounted at the end of the barrel. Four measurements are taken from the first ring as a copper

FIGURE 7

Debris from AWE gas gun experiments.

FIGURE 8

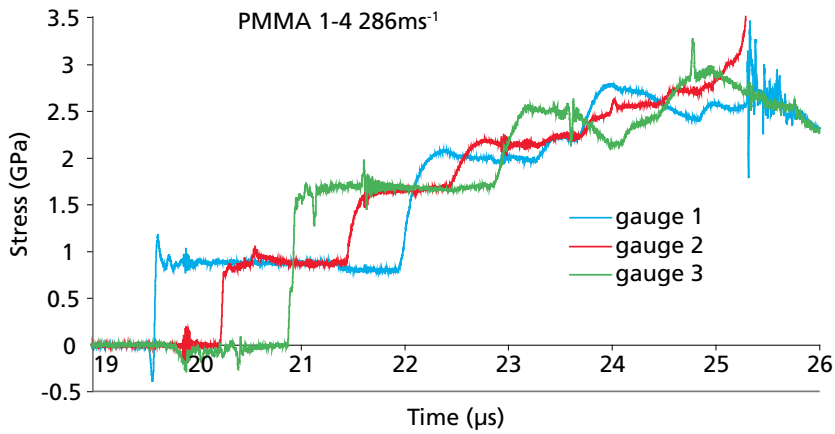

Manganin gauge data.

Despite their minimal thickness embedded gauges do perturb the stress state. This is seen in high shock impedance materials, e.g. metals, which are poorly matched to the plastic insulating layers that make up the bulk of the gauge package. Doppler shifting of laser light by a moving surface provides a nonintrusive way of making velocity measurements of the back surface of a sample or the velocity of an interface with a transparent window material.

flashing on the polycarbonate sabot contacts the pins and completes the circuit. Signals from these pins are used to trigger other diagnostic channels. The second set of four pairs of pins is 10 mm from the first set to make the velocity measurement. Electrical pins can also be used in the targets to measure the arrival of shock waves and check the tilt of the flyer plate at impact.

If the target is constructed from two or more discs of sample material then it is possible to use embedded thin film (100 μm) stress gauges such as manganin or polyvinylidene difluoride to determine the stress state in the sample.

Figure 8 shows typical data from an embedded manganin gauge experiment where the target was two thin discs of polymethylmethacrylate (PMMA) sandwiched between copper anvil plates. The three gauge traces show how the shock wave reverberates between the two copper plates, increasing the stress level in the PMMA with time. This data can be used to develop and validate a hydrocode model for the equation of state of the sample material.

"Electrical pins can also be used in the targets to measure the arrival of shock waves and check the tilt of the flyer plate at impact."

FIGURE 9

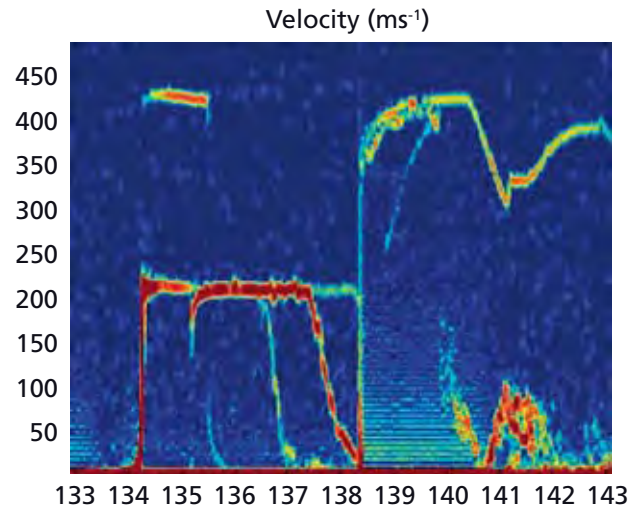

Data from Gas Gun experiment using a PMMA sample and the Het-V.

Box 1

Shock Physics and Equation of State

The AWE gas gun is used to generate shock waves in sample materials. A shock wave is a discontinuous jump in the standard state variables of pressure (P), specific volume (V) internal energy (E) and density (ρ) that moves through the sample at shock velocity (U_s) and accelerates the material to a particle velocity (u_p). For a shock in any material conservation of mass, momentum and energy must be observed across the shock jump. With subscripts of 0 to indicate the variable state ahead of the shock these three conservation laws can be written as:

Conservation of mass: $\rho_0 U_s = \rho(U_s - u_p)$

Conservation of momentum: $P = \rho_0 U_s u_p$

Conservation of energy: $Pup = \rho_0 U_s (E - E_0 + u_p^2/2)$

These equations can be combined to give the Rankine Hugoniot relationship which defines a surface in P,V,E space given that specific volume (V) is equal to the inverse of density ($^1/\rho$).

$$E - E_0 = \tfrac{1}{2}(P + P_0)(V_0 - V)$$

For strong shocks $P >> P_0$ and E_0 is set to zero so this simplifies to

$$E = \tfrac{1}{2}P(V_0 - V)$$

This surface represents all the states that can be reached by a single shock jump and is independent of material. All materials have their own unique equation of state surface in P,V,E space for all states and this can be plotted with the Rankine Hugoniot relation. Where these surfaces cross defines a locus of points known as the principal shock Hugoniot, as shown in the figure below. The principal Hugoniot defines the states achievable in that material with a single shock jump. The AWE gas gun is used to determine shock Hugoniots and information on the equation of state of sample materials.

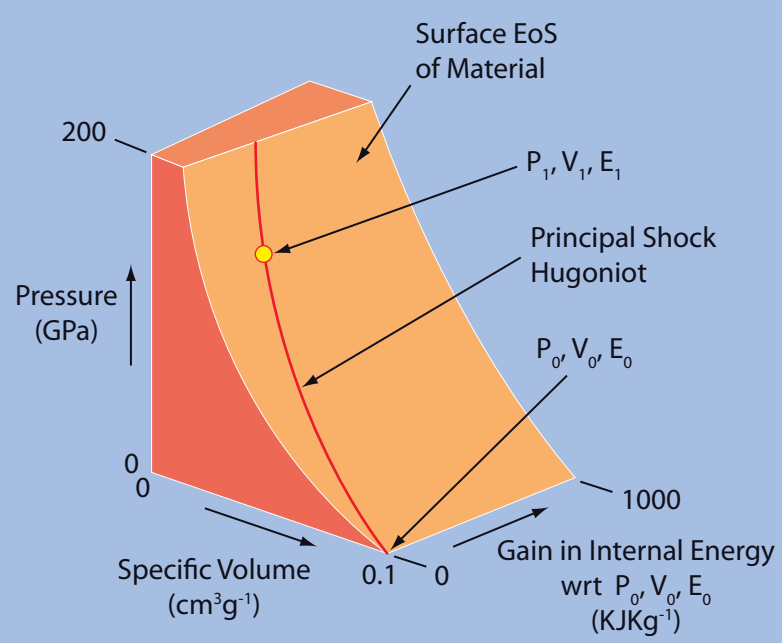

The Het-V (Heterodyne Velocimetry System) developed at AWE can be used to perform measurements by direct interference of the Doppler shifted and unshifted laser light.[2] The Het-V system is used on the gas gun with the optical fibre and lens mounted on an additional ring behind the sample.

Data from a Het-V experiment involving a PMMA sample is shown in Figure 9. The figure shows a simple flat topped shock wave travelling into the PMMA with a particle velocity of just over 200 ms^{-1}. The sample was constructed from several discs of PMMA and additional signals are recorded as the shock reaches each interface before the free surface of the PMMA is reached and the free surface velocity jumps to over 400 ms^{-1}. PMMA shock properties are often used to deduce the particle velocity in a sample.

Conclusion

The AWE single stage gas gun is a versatile shock physics tool which has been used to investigate the equation of state, dynamic strength, porous response and material failure of a range of materials. To date nearly 250 shots have been fired supporting these areas since the gun was commissioned at the end of 2005, with a typical firing rate of one shot a day and a maximum rate of three shots per day for very simple experiments. Future work will include examining the effects of dynamic friction and material phase and microstructure changes under shock loading.

Acknowledgements

The author would like to thank Peter Keightley for providing the bulk of the figures and reviewing this article.

References

1 J. W. Lethaby and W. A. Bailey, Development of a New 70mm Gas Gun, AWRE O, 39/78, (1978)

2 A. Critchley, Optical Velocimetry in Hydrodynamics: a "bright" future, Discovery, Issue 16, (2008)

AUTHOR PROFILE

Peter Taylor can be contacted on e-mail: peter.taylor@awe.co.uk

Peter Taylor • After graduating from Bristol University in 1989 Peter joined the Hydrodynamics division of AWE working on shock and detonation physics research experiments. As well as the gas gun, Peter's research has involved AWE's explosive firing capabilities and a suite of high resolution diagnostics including flash radiography, stress and particle velocity gauges, laser velocimetry and high speed framing and streak cameras. Recently he has been involved in defining the technical specifications for planar impact facilities that will form a core element of the Institute of Shock Physics, the AWE/Imperial College initiative to regenerate fundamental shock physics research in the UK.

Ageing Effects in Plutonium

Like the human body many materials are susceptible to the effects of ageing, which can result in significant changes to their properties and behaviour. One example of this is seen in some polymers, where over time environmental factors such as sunlight, temperature, pollutants, atmospheric oxygen and water can result in discolouration or embrittlement.[1] Another example of a material that can undergo significant microstructural and property changes over time is plutonium (Pu).

Unlike polymers, Pu does not require an external stimulus for the ageing processes to take place. Owing to its radioactive nature it effectively ages "from the inside out".[2] This leads to microstructural changes, the magnitude of which increase with time. The principal decay event in Pu is illustrated in schematic form in Figure 1 and by:

1 $^{239}Pu \rightarrow {}^{235}U + {}^{4}He$

The two products of this reaction each contribute to the generation of lattice damage within the Pu. The α particles (helium nuclei) travel through the lattice acquiring two electrons to form helium (He) atoms. They are highly energetic (5 MeV) and can travel significant distances (up to 10 μm) before coming to rest in the lattice, creating lattice vacancies.

The recoiling uranium (U) atom also travels through the lattice, albeit over shorter distances (~12 nm). Although its energy is lower (86 keV) the damage generated by the uranium atoms is more extensive owing to its larger size. The damage consists of vacancy-interstitial pairs known as Frenkel pairs.

Approximately 2300 Frenkel pairs are created by one U atom. Most Frenkel pairs recombine almost immediately due to the mobility of the vacancies at room temperature; this process is known as "self-annealing". Up to 70% of the Frenkel pairs recombine within 100 pico-seconds after the decay of a Pu atom.[3]

In radiation damage studies of materials the lattice displacement dose is expressed in units of displacements per

FIGURE 1

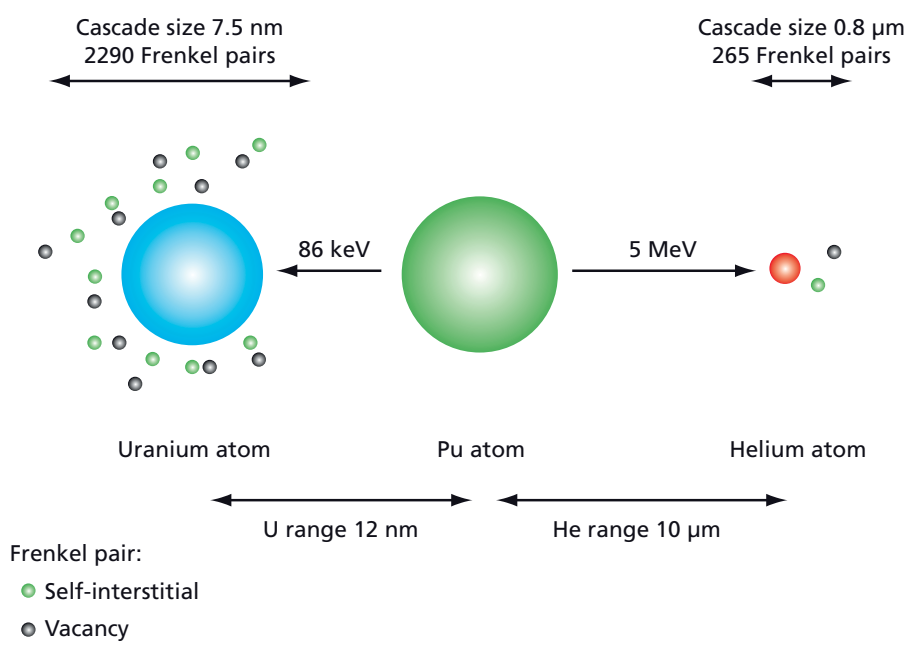

Schematic diagram of the self-irradiation process in plutonium (Pu).

"Unlike the other transmutation products helium has little solubility in the plutonium lattice. However atoms can enter lattice vacancies, enabling them to diffuse through the microstructure."

atom (dpa). For Pu it has been calculated that the lattice damage accumulates at a rate of 0.1 dpa.[4] In 10 years all the atoms will have been moved from their original lattice sites.

The self-irradiation also leads to the accumulation of americium (Am), uranium (U) and neptunium (Np) in the microstructure. It has been estimated that after fifty years of storage plutonium may contain 2000 ppm of He, 3700 ppm Am, 1700 ppm U and 300 ppm Np.[5]

Unlike the other transmutation products He has little solubility in the Pu lattice. However the He atoms can readily enter lattice vacancies, enabling them to diffuse through the microstructure. Over time this migration and coalescence of He atoms results in the formation of bubbles. This phenomenon is not only applicable to Pu. Materials used in nuclear reactors e.g. austenitic stainless steels, have been seen to exhibit steady state swelling of up to 60%, caused by the agglomeration of lattice vacancies.[6]

The issue of He in Pu was first recognised as long ago as 1958 by Dempsey and Kay.[7] They estimated that disintegration of Pu would not occur in less than 100-200 years. More recently Wolfer has suggested that based on the experience of reactor materials, the onset of steady state swelling due to radiation damage may be the life limiting factor for Pu.[3] This may not occur in Pu that is less than 100 years of age.

The aim of this article is to summarise current understanding of He bubbles within Pu and the effects of the bubbles on its mechanical properties.

FIGURE 2

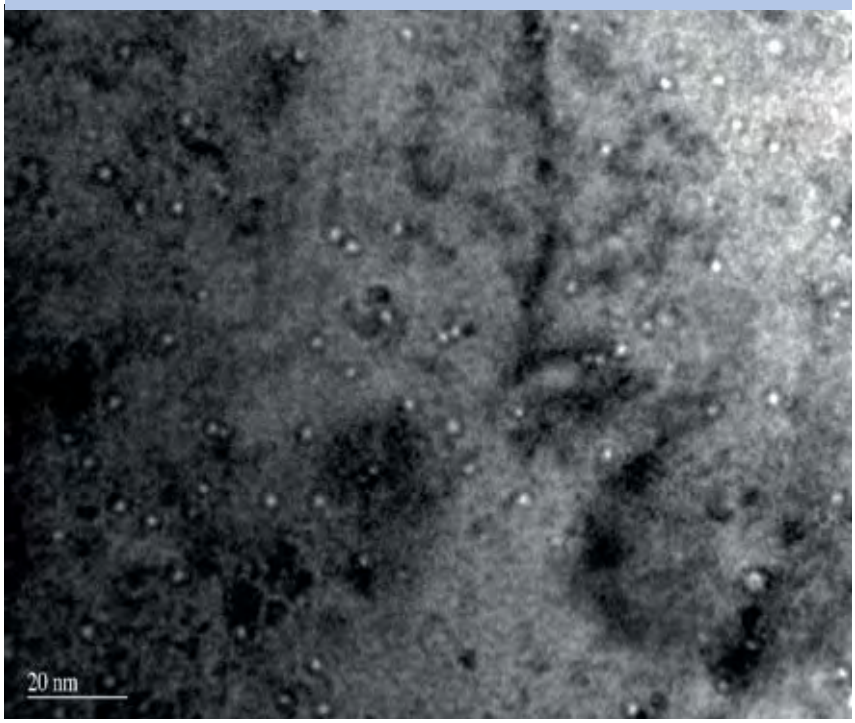

TEM micrograph of 17-year-old Pu stored at ambient temperature.

Transmission Electron Microscopy

The evolution of He bubbles in Pu has been studied by researchers at Lawrence Livermore National Laboratory using transmission electron microscopy (TEM).[8] Figure 2 shows a TEM micrograph of 17 year old Pu stored at ambient temperature. The He bubbles appear as small white dots of approximately 1-2 nm in diameter. Studies using TEM indicate that mean bubble density increases with age; however the mean bubble diameter is largely unchanged. Bubbles with diameters smaller than 0.7 nm can not be resolved by TEM.

Considerable care is required in the interpretation of the images. The absence of a large strain field associated with the bubbles can render them invisible when viewed in focus. This problem can be overcome by a technique known as Fresnel fringe imaging, by which the bubbles are observed in the under- and over-focus conditions.

Bubble measurement is highly dependent on the skill of the operator to differentiate between genuine bubbles and

FIGURE 3

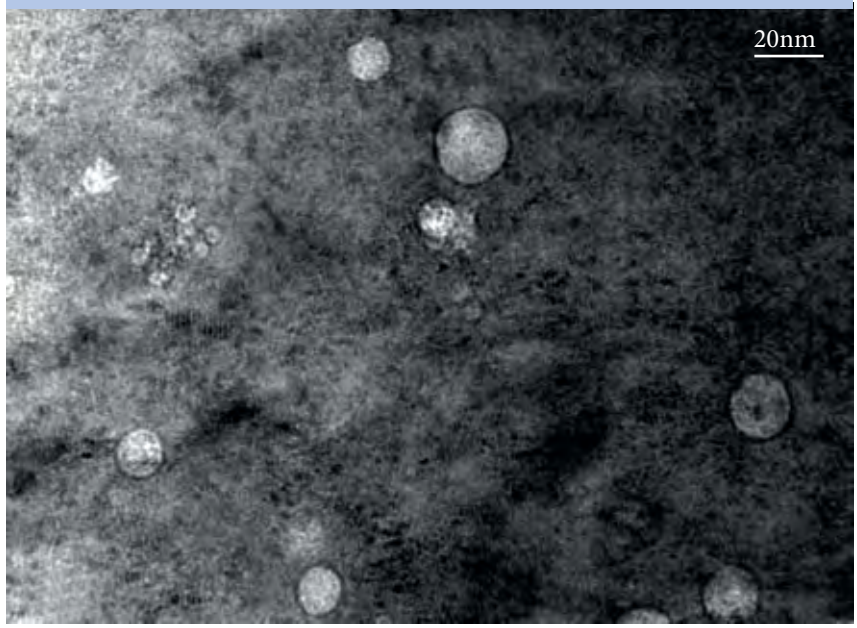

TEM micrograph of 42-year-old Pu heated to 425°C showing bubbles with a mean diameter of 11 nm.

FIGURE 4

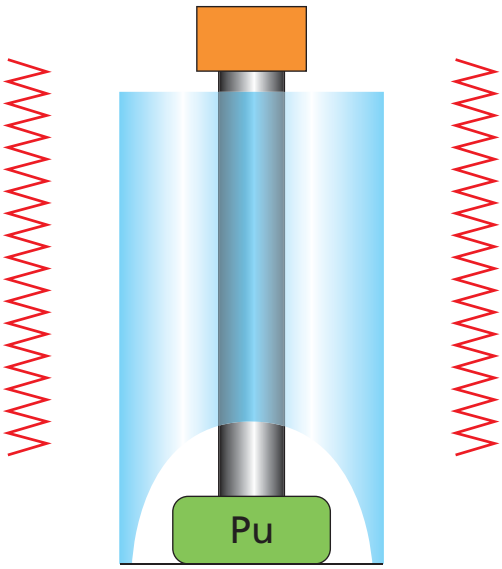

Schematic diagram of a dilatometer setup (left). An LVDT probe resting on a specimen (right).

"When plutonium is heated, the observed contractions are thought to have been caused by the annealing out of the accumulated radiation damage present in the lattice."

surface artefacts induced by specimen preparation. The bubbles in an under-focused image appear as a dark fringe surrounding a light dot, while in an over-focus image they are light fringes surrounding a dark dot. The image in Figure 2 was taken in the under-focused condition.

When the Pu is heated bubble growth occurs and the bubbles are easier to observe owing to the greater strain contrast. Figure 3 shows a 42-year-old Pu specimen heated to 425 °C. The heat treatment has caused the bubbles to expand to a mean size of 11 nm. The expanded bubbles also induce a larger strain in the adjacent lattice making the Fresnel fringe technique unnecessary.

Although TEM has shown the sizes of He bubbles in Pu stored at ambient temperature are only 1-2 nm, the possibility that these bubbles may expand in future causing macroscopic swelling cannot be excluded. One technique by which the evolution of radiation damage and He bubbles in aged Pu may be evaluated is by dilatometry.

FIGURE 5

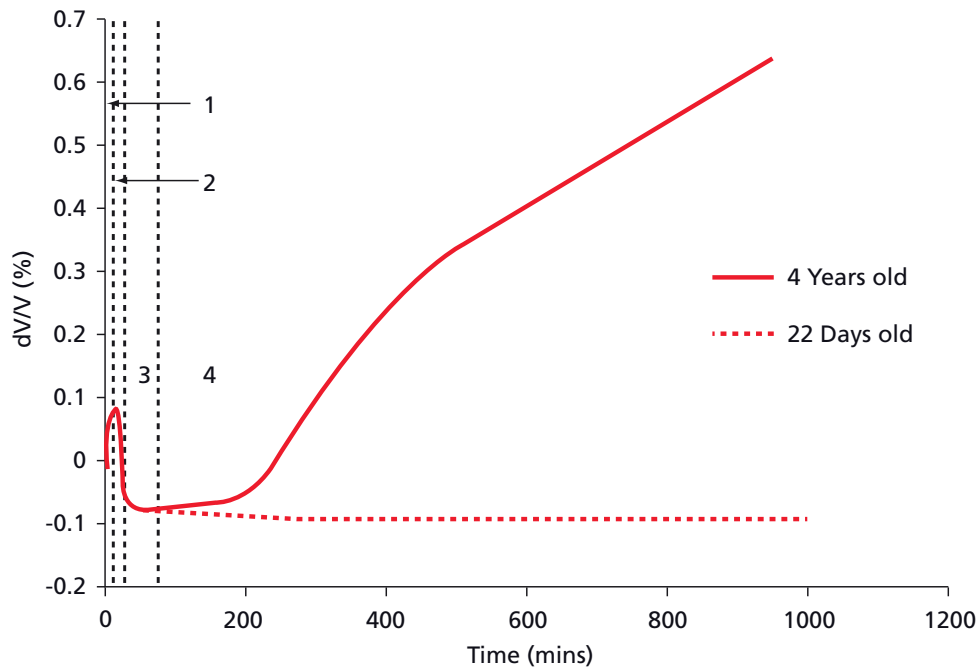

Dilatometry trace of 22 days old and 4 year old Pu subjected to an isothermal treatment to 300°C. The four stages of behaviour are annotated on the 4 year old trace.

Dilatometry

Dilatometry monitors dimensional changes of specimens with respect to temperature and/or time. In a dilatometer the specimen is placed inside a quartz tube which is mounted inside a furnace and a probe rests on its upper surface, as shown in Figure 4. The probe is connected to a linear variable displacement transducer (LVDT) which measures any changes to the specimen dimensions during the experiment. Probe position can be plotted against time or temperature and is continuously recorded throughout the experiments.

Pu specimens were subjected to elevated temperatures for extended periods of time in order to study the growth of the He bubbles.[9] Figure 5 compares traces from dilatometry runs for Pu aged 4 years and 22 days. The changes in probe position are normalised volume changes and are plotted against time.

The trace in Figure 5 shows four distinct stages. The first stage occurs as the specimen heats to the desired temperature and is a function of the thermal expansion coefficient of the material.

Once the treatment temperature has been attained

FIGURE 6

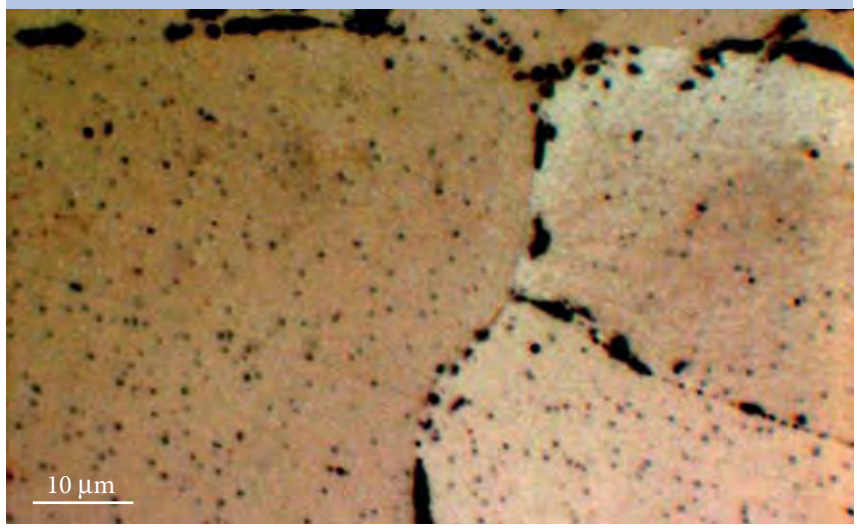

Optical micrograph of 31-year-old Pu heated to 300°C for 306 hours showing a network of micron-sized bubbles distributed throughout the microstructure.

FIGURE 7

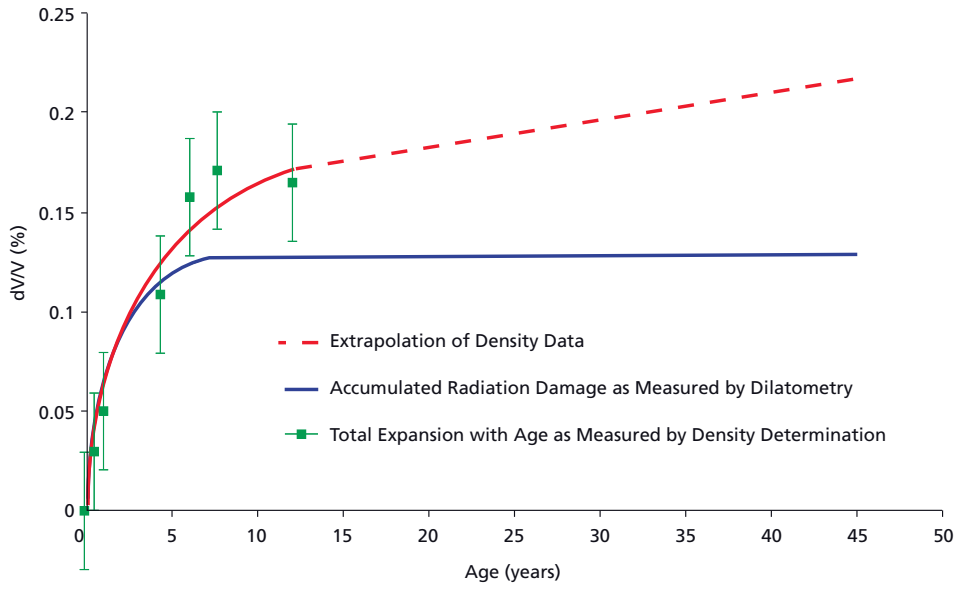

Graph showing the increase in volume (calculated from the dilatometry data) with age of Pu.

FIGURE 8

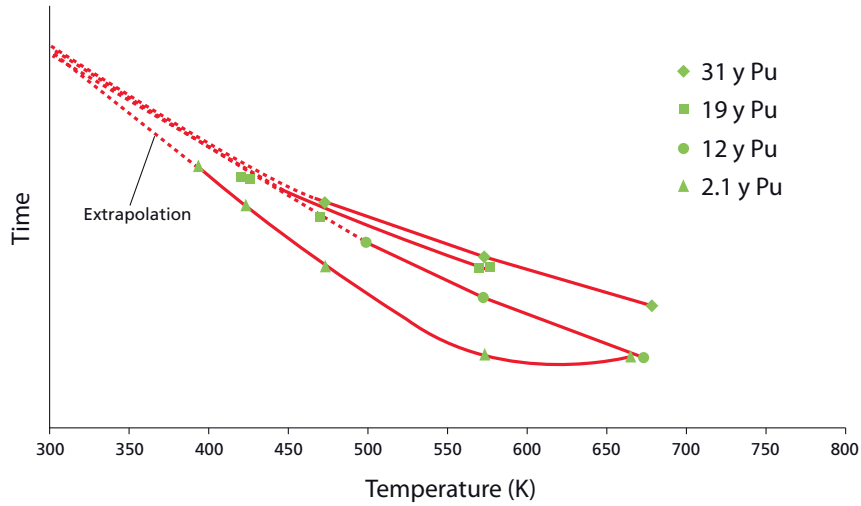

Extrapolation of incubation times to ambient temperature to predict the time required before swelling begins to occur.

the second stage, contraction of the specimen, may be observed. The length of time over which this contraction occurs is dependent on the test temperature. At 150 °C the contraction was observed to continue for approximately 33 hours, while at 400 °C it was only 5 minutes. As a consequence these contractions cannot be ascribed to differences in expansion due to temperature gradients within the dilatometer during heating. It is thought that they have been caused by the annealing-out of the accumulated radiation damage that is present in the lattice. The extent of this contraction enables the amount of radiation-induced lattice damage to be measured. As shown in Figure 5 this is dependent on the age of the specimen.

The third stage of the graph is the incubation period where no change in volume is observed. During this stage He bubbles, which are a product of the radioactive decay process and subsequent diffusion of He atoms, are redistributed from their original network into a new thermodynamically-stable embryo network at the test temperature.

This process then leads to the fourth stage where subsequent expansion of the material occurs as the embryos grow in size. At this stage further differences in the dilatometry response of Pu specimens of different ages are apparent.

The significantly higher levels of He in older material cause it to exhibit subsequent expansion once the radiation has been annealed out. This is in contrast to 'un-aged' material, which has a negligible amount of He present.

Metallographic examination of the dilatometry specimens revealed the presence of a network of micron-sized

"The significantly higher levels of helium in older material cause it to exhibit subsequent expansion once the radiation has been annealed out."

FIGURE 9

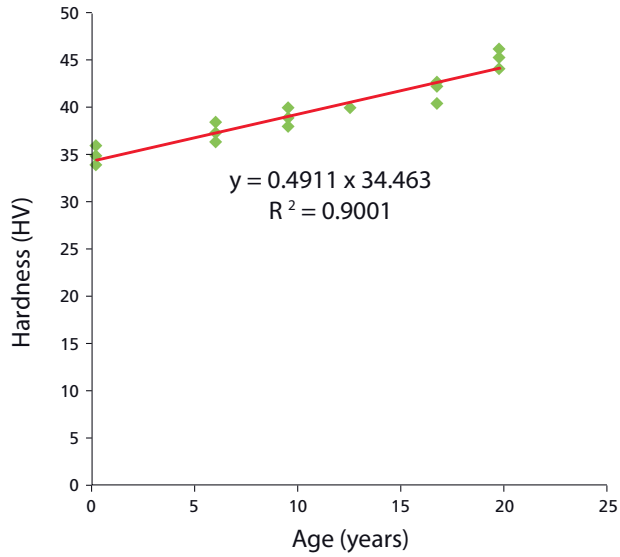

Graph showing the variation in Vickers hardness (HV) with age for Pu.

bubbles. Figure 6 shows a 31 year old Pu specimen which has been heated to 300 °C for 306 hours. He bubbles are situated at both the grain boundaries and within the grains themselves. Specimens heated to higher temperatures have shown larger bubbles.

In order to eliminate specimen preparation as a cause of these bubble networks specimens are examined in both unetched as well as the etched condition. The observation of these bubble populations in both conditions indicates that their existence cannot be attributed to the effect of etching the Pu during specimen preparation.

From the bubble diameters and densities observed from metallography the rate of diffusion through the Pu lattice can be calculated by

$$D = 7.58 \times 10^{-12} \exp\left(\frac{-Q}{RT}\right) \quad (2)$$

This calculation assumes that the bubbles in aged and heat-treated Pu can be considered as a collection of hollow spheres. D is the diffusion coefficient, which is expressed in units of $m^2\ s^{-1}$, R is the gas constant (8.31 J $mol^{-1}\ K^{-1}$) and T is the temperature in K. The activation energy (Q) of 86.34 kJ mol^{-1} is close to that measured for Pu self-diffusion (99.6 kJ mol^{-1}). This indicates that He does not diffuse interstitially through the Pu lattice but as He occupied vacancies.

The magnitude of the contraction after reaching the treatment temperature (stage two) can be used to calculate

"Swelling has been determined in plutonium of up to 42 years of age where, after an initial 4-5 year period of rapid expansion, a plateau region is observed."

"The increase in hardness with age is attributed to the presence of helium bubbles defects ensuing from radiation damage."

the swelling due to the accumulation of radiation damage with age. This has been determined in Pu of up to 42 years of age where, after an initial 4-5 year period of rapid expansion, a plateau region is observed. This is shown in Figure 7. This period of stasis occurs when the rate of defect generation equals the rate of annihilation and can be shown to represent a defect concentration of approximately 6%. It is also clear that void swelling is not apparent over this timescale.

The overall swelling with time can also be monitored by density measurement. To date these changes have only been measured on Pu up to 12 years of age. Extrapolation has been accomplished by adding the known expansions due to the generation of He bubbles and other transmutation products (Am, U, Np).

The lengths of the incubation times as a function of temperature can be extrapolated down to ambient temperature to identify the completion of He bubble nucleation and the onset of bubble growth. Figure 8 shows extrapolated incubation times. The data suggest that this has been estimated to of a similar order to that suggested by Wolfer.[3] There may be other factors that could alter this estimate and further work is required in order to corroborate this hypothesis.

Effects of Ageing

The effect of radiation damage has been extensively studied in order to ascertain its effect on the mechanical properties of metals and alloys. A number of studies have shown that the presence of He reduces the ductility and fracture toughness of stainless steels, while the hardness, yield and tensile strengths are increased. The effect of He is more significant on long term deformation especially creep and fatigue at elevated temperatures. The damage levels and He contents generated are far in excess of what is seen in Pu.

The relatively modest levels of radiation damage in Pu have been observed to increase its hardness with age, as shown in Figure 9. This increase is attributed to the presence of He bubbles and defects ensuing from radiation damage. These act as an impediment to dislocation motion resulting in a strengthening of the lattice.

For many metals the yield stress of a material is approximately one-third of its hardness. It can be inferred that some of the products of the ageing process have resulted in an increase in the strength of the Pu.

The consequences of radiation damage in aged Pu extend beyond lattice damage and He bubbles. Another possible consequence of the evolution of lattice damage in Pu is the change to the diffusion characteristics of the material. Such changes could affect the phase stability of the Pu by lowering the activation energy required for diffusion.This radiation enhanced diffusion may also affect the behaviour of other elements present in the material.

There are many aspects of the behaviour of Pu that remain to be fully understood. Pu research continues to offer a stimulating and thought-provoking field in which to work.

Acknowledgments

The authors wish to thank colleagues in the Actinide Materials Group for their assistance during the experimental work described in this article.

Figures 2 and 3 are reproduced with permission of Dr A Schwartz, Lawrence Livermore National Laboratory.

References

1 J. J. Murphy, M. Patel, J. M. Yorke, Discovery, 10 (2005), 2-13.
2 S. S. Hecker, J. C. Martz, Proc. Int. Conf. Ageing Studies and Lifetime Extension of Materials (ed. L. G. Mallinson), Kluwer Academic Publishers (1999), 23-52.
3 W. G. Wolfer, Los Alamos Science, 26 (2000), 274-285.
4 A. Arsenlis, W. G. Wolfer, A. J. Schwartz, J. Nucl. Mater., 336 (2005), 31-39.
5 S. S. Hecker, Metall. Mater. Trans. A, 39 (2008), 1585-1592.
6 F. A. Garner, W. G. Wolfer, J. Nucl. Mater., 122/123 (1984), 201-206.
7 E. Dempsey, A. E. Kay, J. Inst. Met., 86 (1958), 379-384.
8 A. J. Schwartz, M. A. Wall, T. G. Zocco, W. G. Wolfer, Phil. Mag., 85 (2005), 479-488.
9 D. W. Wheeler, P. D. Bayer, J. Alloy. Compd., 444-445 (2007), 212-216.

AUTHOR PROFILE

Peter Bayer can be contacted on e-mail: peter.bayer@awe.co.uk

Peter Bayer • Peter joined AWE in November 1958 as a scientific assistant. Over the years he has worked in a diverse range of subject areas including fuel element production, fibre-reinforced composites, plasma-sprayed coatings, thick film technology for electronic applications and, most recently, plutonium research. He retired as a principal scientist in August 2007 but continues to work part-time as a consultant. He is a chartered engineer and a member of the Institute of Materials, Minerals and Mining.

AUTHOR PROFILE

David Wheeler can be contacted on e-mail: david.wheeler@awe.co.uk

David Wheeler • David graduated from the University of Surrey with a BEng(Hons) degree in materials technology. This was followed by an MSc in non-destructive testing from Brunel University and a PhD in mechanical engineering from the University of Southampton. He joined AWE in February 2003 in the Actinide Materials Group (Materials Science Research Division) to work on plutonium metallurgy. He is a chartered engineer, a member of the Institute of Materials, Minerals and Mining and is the author of more than twenty publications in the scientific literature.

The Achievements of Radioactive Waste Assay

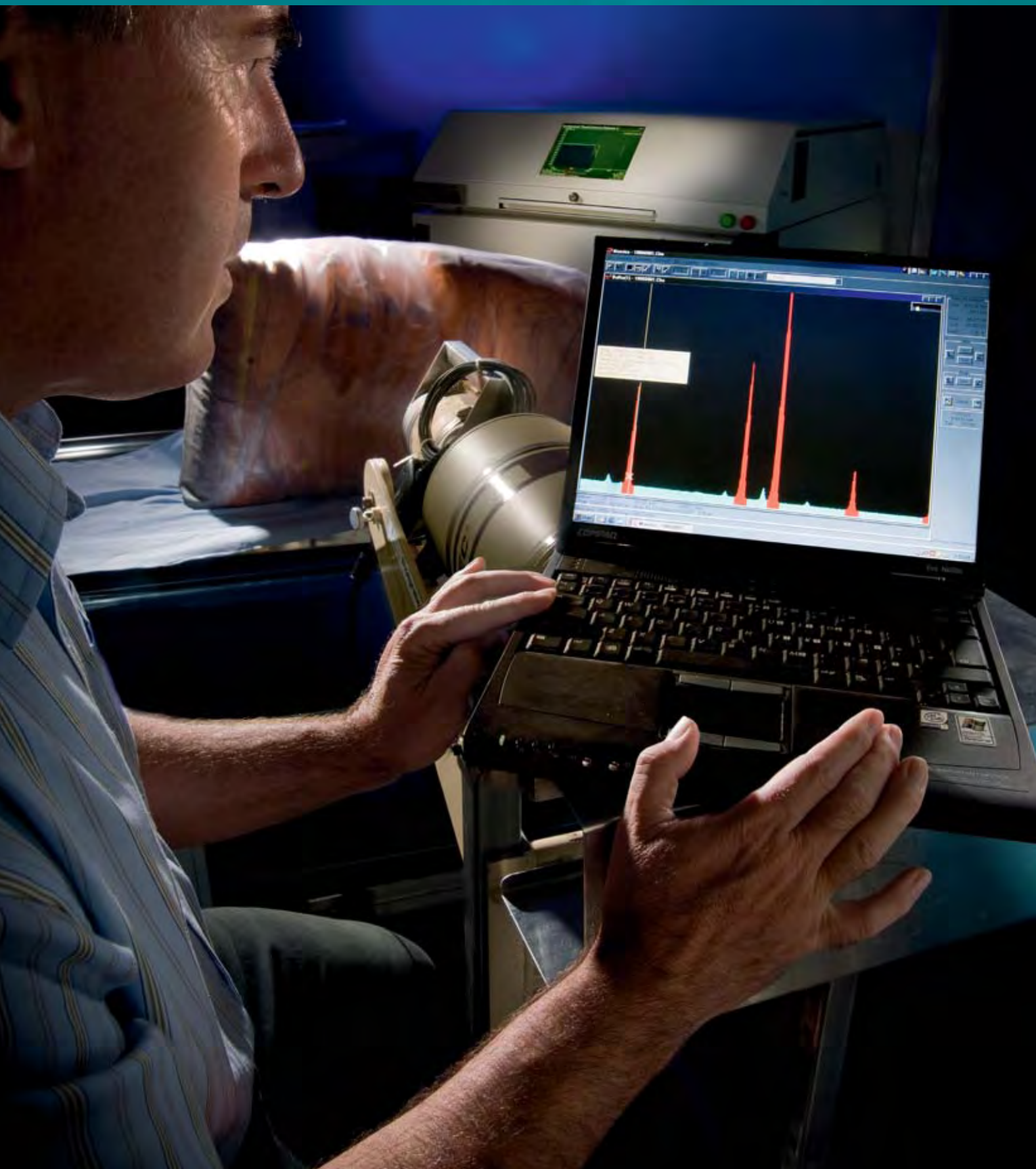

The full life cost to dispose of a 200 litre drum of solid radioactive Intermediate Level Waste (ILW) exceeds £40,000. AWE has made considerable efforts to reduce the amount of ILW it generates and classify legacy, operational and decommissioning waste-streams at lower categories; such as Low Level Waste (LLW), Low Level Waste Drigg (LLWD), Very Low Level Waste (VLLW) and Exempt Waste (EW). High Level Waste (HLW) is not produced at AWE.

There are big cost incentives to minimise waste volume and classify it at the lowest level possible. Furthermore, the LLW repository at Drigg is a finite national resource and will only accept waste that meets its strict Conditions for Acceptance (CFA). In the case of plutonium (Pu) contaminated waste this must be within the narrow activity range of 0.4-100 Bq g^{-1} alpha. This equates to 0.008-2 mg Pu in a 200 litre waste drum, which is beyond the detection limits (DL) of many waste assay options.

Table 1 summarises the disposal routes, costs and activity ranges for each waste category and the main radioactive contaminants encountered at AWE. These include alpha emitters such as Pu, enriched uranium (EU) and depleted uranium (DU) and beta emitters such as tritium (H^3), caesium (Cs^{137}) and cobalt (Co^{60}).

Best Practical Means (BPM) studies have been undertaken in order to identify the most appropriate radioactive waste assay technique for each waste category and contaminant combination. Box 1 summarises the BPM study for DU waste assay together with potential interferences for the principle assay options. Subsequent trials, using waste drum or package standards containing traceable sources, have confirmed acceptable measurement accuracy and DL for the assay option selected.

TABLE 1

Category	Activity range (Bq g^{-1})	Disposal route	Disposal cost (£ per 200l drum)
ILW	> 4,000 Pu, EU, DU > 12,000 beta	Indefinite storage at AWE until a national ILW repository is available	40,000
LLW	< 4,000 DU, EU < 12,000 beta	LLW repository at Drigg	250
LLWD	< 100 Pu	LLW repository at Drigg	250
VLLW	< 4	As authorised	50
EW	< 11.5 DU, EU < 0.4 Pu	As AWE policy dictates	20

Activity ranges, disposal routes and costs for the main radioactive contaminants and waste categories encountered at AWE.

Pu Waste Assay

An article entitled 'Waste Assay the Challenge' was published in Discovery Issue 8 (February 2004). That article highlighted the feasibility of meeting the stringent Drigg CFA criteria by measuring the high yield, but relatively low energy, 60 keV photon from americium (Am^{241}) in-growth using passive High Resolution Gamma Spectrometry (HRGS). This technique was cautiously applied to low bulk density and low atomic number (Z) wastes because of low gamma-ray transmission at 60 keV. The initial work has resulted in over 2,000 drums and 1,000 HEPA filters being reclassified from a provisional assignment of ILW to LLWD.

Subsequent inter comparison studies on progressively denser (higher Pu content and higher Z) waste drums gave consistent results for the Am^{241} signature and much more penetrating, but lower yield, emissions such as the 414 keV photon from Pu^{239} and fast neutrons from Pu^{240}, see Figure 1.

FIGURE 1

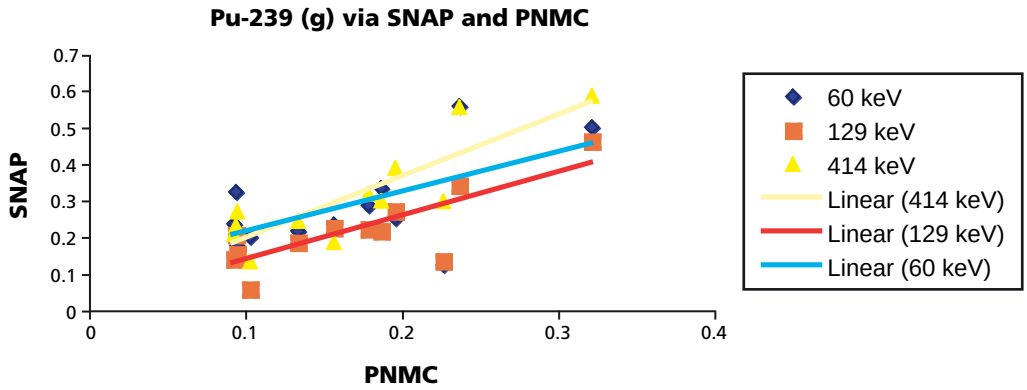

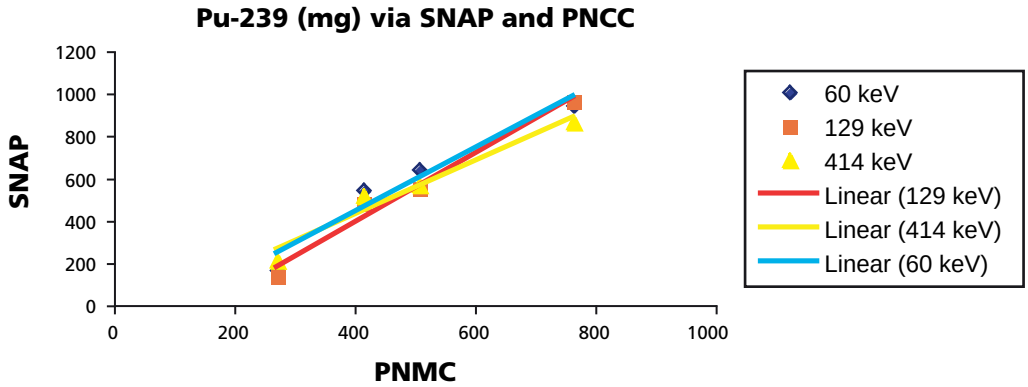

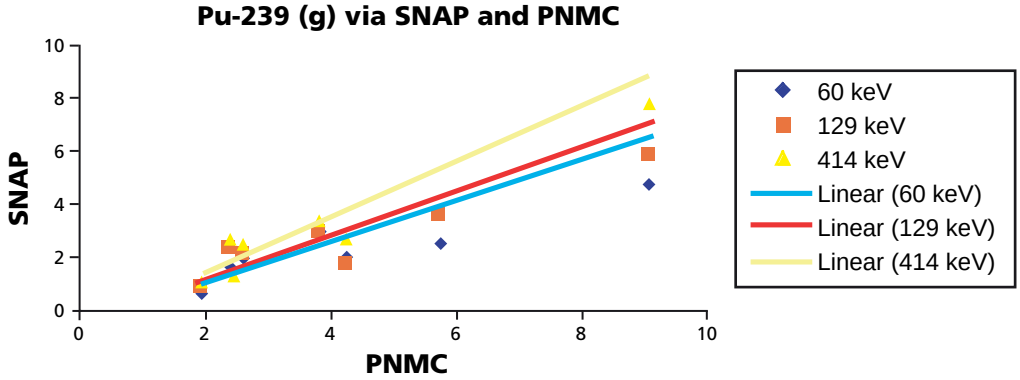

Inter-comparison studies on progressively denser and higher Pu content drums between neutron counting techniques (PNCC and PNMC) and SNAP at all photon energies.

FIGURE 2

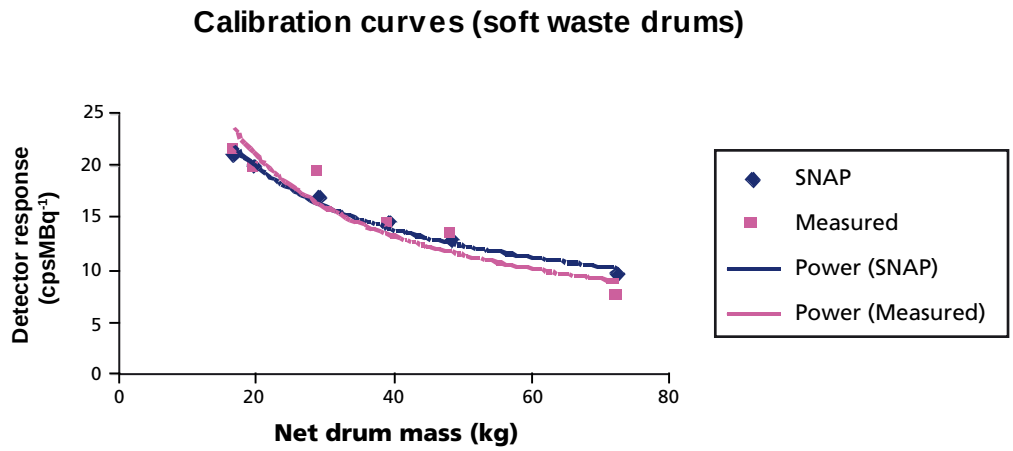

Experimentally derived calibration curve for Am^{241} in low Z waste drums, using SNAP, compared to the measured responses.

This work has increased the potential to include the more challenging waste streams that were previously believed to be too difficult to assay accurately. The range of applicability of the original HRGS technique has been extended to cover the entire range of waste package types, encountered at AWE, by using Spectral Non-destructive Assay Platform (SNAP) analytical software. SNAP corrects the HRGS detector calibration for counting geometry, e.g. package size and distance from detector, and gamma- ray attenuation, e.g. shielding, matrix density and composition. It also has routines for Differential Peak Analysis (DPA) and Pu and DU/EU Lump Corrections so that all gamma-ray signatures from a given isotope yield consistent results.

The validity of SNAP has been demonstrated for a diverse range of waste package types, isotopes, activity ranges and waste streams by measurements on standard substances with known amounts of activity. Figure 2 shows that experimentally derived calibration curves were similar to those computed by SNAP. The SNAP calibration curves take minutes to be generated compared with days for conventional measurement techniques.

AWE has also participated in a comparison of procedures used at UK nuclear sites for gamma assays of potentially contaminated or activated materials. This involved the 'blind' assay by several establishments of a National Physical Laboratory certified waste drum containing Am^{241}, Cs^{137} and Co^{60} at EW levels. The SNAP results reported 95 % of the true activity for Cs^{137}, 94 % for Co^{60} and 81 % for Am^{241}. The SNAP performance was amongst the best reported.

EU Waste Assay

The performance of SNAP has also been compared with the Segmented Gamma Scanner (SGS), which represents a benchmark technique for accuracy amongst the gamma-ray based waste assay options. Both systems use a similar HRGS detector with the waste drum located on a rotating turntable to reduce uncertainties associated with non-uniform activity and matrix distribution. The SGS detector is positioned relatively close to the waste drum wall and scans the whole drum, from top to bottom, pausing at eight equally spaced drum segments. A transmission measurement, across each segment, is used to

FIGURE 3

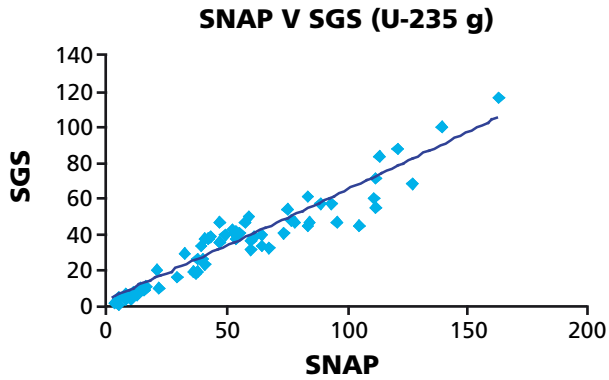

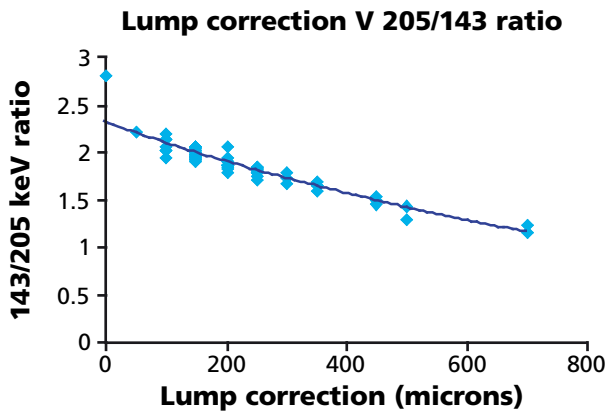

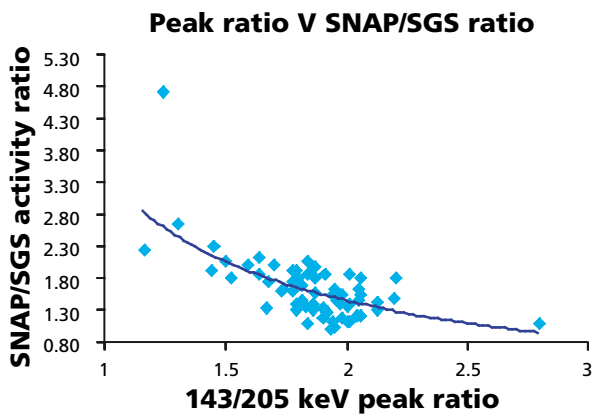

SNAP and SGS results for the most active EU drums.

FIGURE 4

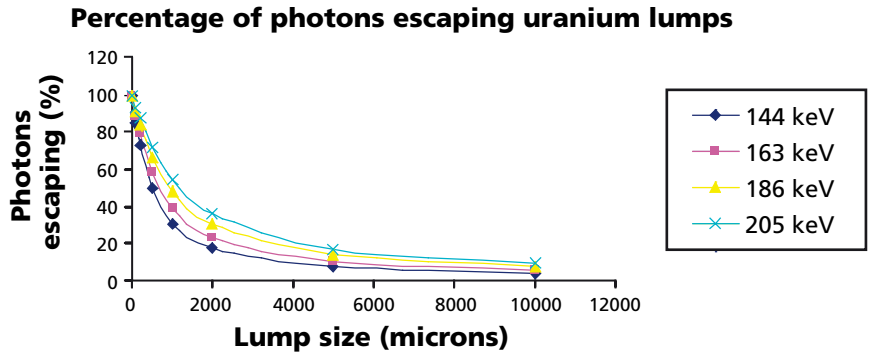

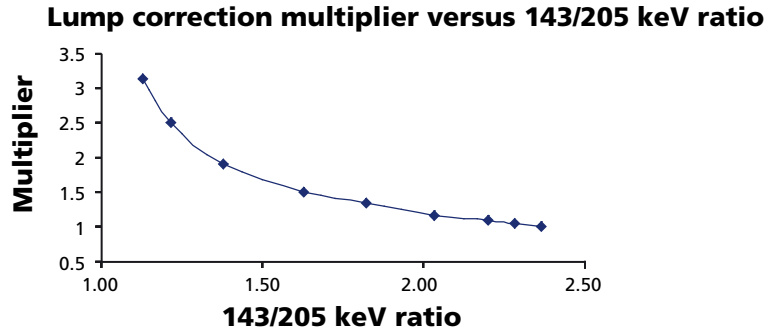

Low energy photon emission sharply drops off with increasing uranium lump size so that rapidly increasing lump correction multipliers need to be applied as the 143/205 keV ratio falls.

correct the detector calibration for matrix density.

In contrast the SNAP detector is positioned further away so that the whole drum is counted continuously and transmission measurements are not normally employed. This methodology results in improved detection limits and shorter counting times with SNAP compared to SGS. However, it needed to be demonstrated that this improved performance did not come at the expense of accuracy. Initial trials showed that the SGS progressively underestimated EU for drum standards containing increasingly larger lumps of EU. This error correlated with a progressive reduction in the 143/205 keV peak area ratio. Increasingly large SNAP lump corrections were required in order to obtain consistent results that agreed with the known EU activities at all photon energies. Subsequent measurements, on the most active EU waste drums generated at AWE, gave similar observations. Figure 3 summarises the results in graphical form. SNAP results correlated reasonably well with the SGS but averaged around 50 % higher due to the need for small U lump corrections that were not performed by the SGS. The need for lump corrections was flagged by abnormally low 143/205 keV ratios. There was a good correlation between the size of the uranium lump correction required to obtain consistent results at all the principle U^{235} photon energies; 143, 163, 185 & 205 keV and for the 143/205 keV ratio. As the 143/205 keV

"The SNAP results reported 95 % of the true activity for Cs^{137}, 94 % for Co^{60} and 81 % for Am^{241}. The SNAP performance was amongst the best reported."

ratio increased, from just over 1:1 to over 2:1, the agreement between SNAP and SGS improved. This result indicated that the average matrix density used by SNAP was equivalent to the transmission corrected density used by SGS. This is because the 143/205 keV ratio is relatively unaffected by waste composition, e.g. paper or steel, but drops rapidly with increasing uranium lump size.

It is worth noting that the lump correction routine rapidly saturates because 'infinite thickness' for gamma-ray transmission in U is only a few mm at low photon energies, 185 keV for EU, compared to several cm at higher energies, 1001 keV for DU. The curves in Figure 4 illustrate just how sharply photon emissions and 143/205 keV ratios from EU drop off with increasing uranium lump size. Rapidly increasing lump correction multipliers are required to overcome this problem. In the case of AWE wastes the need to perform lump corrections was relatively rare and normally a small correction of only a few hundred microns was sufficient.

DU Waste Assay

SNAP has been applied to the most challenging heterogeneous, high bulk matrix density, high mass, high Z, high DU mass waste streams encountered at AWE. Figure 5 shows a typical pre- and post-trial detonation. The waste is collected and shredded. Larger, non-shredable, material is placed in the bottom of the waste drum and the smaller material is placed on top. Each trial generates around 20 drums of waste.

The SGS was only used to assay the lighter, non-grouted drums and underestimated the expected DU content by a factor of around two. This error was attributed to the transmission measurements indicating low matrix density, for the most active drum segments, because lump corrections, at 1001 keV were negligible.

In contrast the SNAP results correlated reasonably well with the SGS; they were around a factor of 2 higher and averaged within 30 % of the DU mass used in the firings.

It is possible to rationalise the underestimation by SGS, compared to SNAP, as follows:

- Large and dense items occupy relatively low volumes within the waste drum compared to the equivalent mass of lower Z materials
- Most of the activity in the drum will tend to be associated with the less dense regions because of the larger surface area to volume ratio. In these circumstances the SGS transmission measurements will associate low matrix density with high activity and underestimate. The overall drum matrix density used by SNAP tends to average out these effects

This hypothesis was supported by the observation that sources located within low density regions in heterogeneous drum standards were underestimated by SGS compared to measurements at high density locations. Less variation was obtained when the same measurements were made using SNAP.

FIGURE 5

Pre- and Post-trial detonation pictures.

FIGURE 6

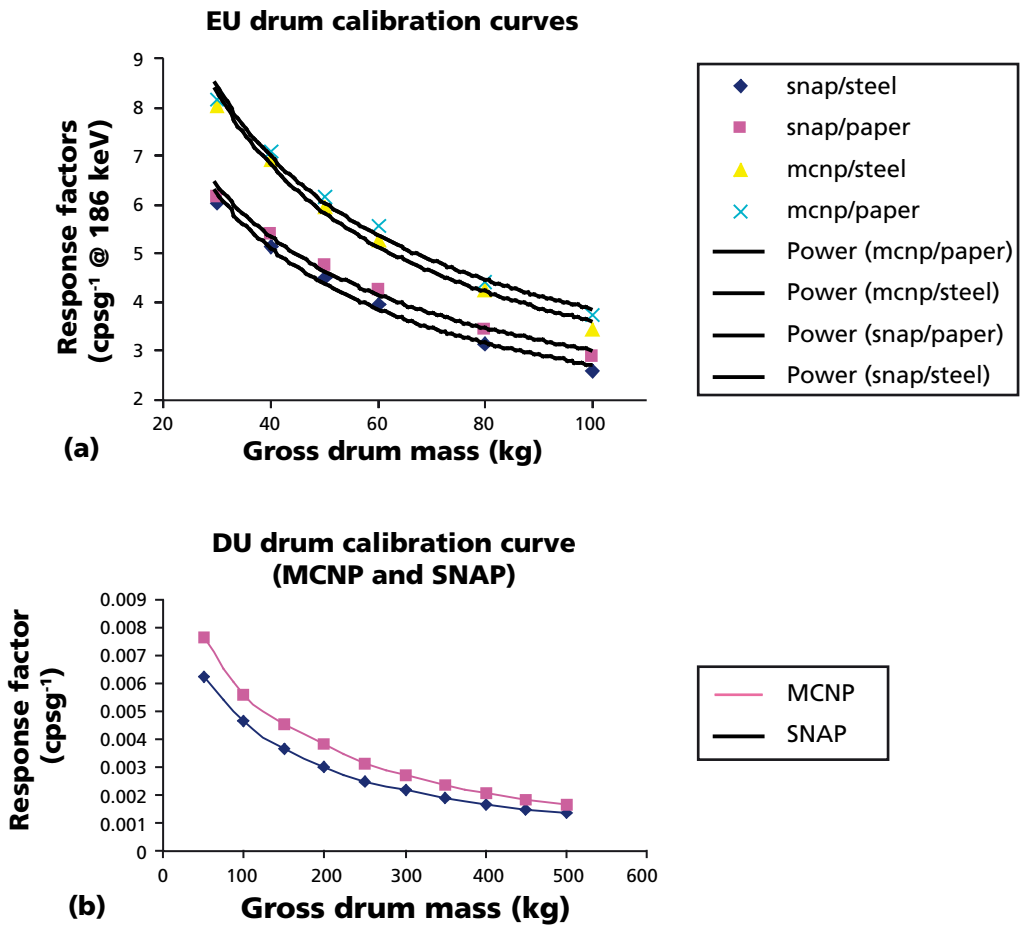

Comparison of MCNP calibration curves and SNAP computed curves with different materials for EU waste (a) and DU waste (b).

Monte Carlo N Particle (MCNP) code calculations were used to confirm the shapes of the calibration curves, generated by SNAP for U waste assay. Figure 6 illustrates the comparative curves. Little difference was observed between paper and steel calibration curves, even at the lower photon energies such as 185 keV, but the MCNP curves were around 20 % higher than those from SNAP. This difference was because the active volume of the gamma ray detector crystal was less than its physical dimensions due to effects such as imperfect electrical field strength.

In many DU facilities it has been established that a large proportion of wastes, provisionally classified as LLW, can be readily reclassified as EW by using SNAP and short counting times. This reclassification can be made because of the much higher 11.1 Bqg^{-1} threshold, applicable to DU, compared to the 0.4 Bqg^{-1} threshold used for most other radioactive materials.

Box 1

BPM Study and Assay Interferences

A BPM (Best Practical Means) study starts with an objective e.g. to segregate EW from LLW for DU waste drums. Then all of the cost considerations e.g. time, money, training, maintenance are balanced against performance required e.g. accuracy, detection limit (DL) in order to select the most suitable assay option

Option	Costs	Accuracy	DL	Suitability
Passive Neutron Counting (PNC)	Low	Medium	Poor	No
Passive Neutron Coincidence counting (PNCC)	High	Medium	Poor	No
Active Neutron Counting (ANC)	Very High	High	Good	Too expensive
Segmented Gamma Scanner (SGS) (Low Resolution)	Medium	Medium	Good	Inferior accuracy
Segmented Gamma Scanner (SGS) (High Resolution)	High	High	Good	Too costly and complex
Passive Low Resolution Gamma Spectrometry (LRGS)	Low	Medium	Good	Inferior accuracy
Passive High Resolution Gamma Spectrometry (HRGS) (SNAP)	Medium	High	Good	Yes
Gross gamma activity	Low	Medium	Fair	No
Chemical analysis	Medium	Low	Good	No

Application of the BPM study selected assay option needs to take account of the following potential interferences:

Gamma techniques: Gamma emitters, high bulk density, high Z matrix, internal shielding and self shielding.

Passive Neutron techniques: Neutron emitters, moderators, neutron poisons, self multiplication and light element multiplication.

Active Neutron techniques: Self shielding from the interrogating neutron flux, moderators, poisons, other neutron emitters.

Reactor Waste Assay

SNAP has also been applied to waste streams generated from the decommissioning of the Herald reactor at AWE. These waste streams included heavily shielded drums containing activated reactor components that had been stored at AWE whilst activity levels decayed from ILW to LLW.

Measurements of the Co^{60} content of these packages were used to confirm that they were suitable for off-site disposal. Several hundred waste drums and packages of more lightly activated decommissioning wastes were assayed for a variety of isotopes including Cs^{137}, Co^{60}, Ag^{108}, Zn^{65} and Mn^{56}. The high photon yields and energies from these isotopes reduced measurement uncertainties when compared with measurements of lower energy photons from isotopes such as Am^{241}.

Future Work

The indications are that a high percentage of legacy waste drums at AWE can be reclassified from a provisional assignment of ILW to LLWD and sent for off-site disposal. Robust cases will be prepared to justify reclassification of the more challenging high density, high Z drums.

A waste bag monitor will be procured and commissioned in order to improve detection levels and classify radiation controlled area wastes as EW wherever possible.

SNAP will be considered for accreditation by the United Kingdom Accreditation Service (UKAS) in order to improve customer confidence in quality.

AUTHOR PROFILE

Timothy Miller can be contacted on e-mail: timothy.miller@awe.co.uk

Timothy Miller • Timothy obtained BSc (first class honours) and PhD degrees in Chemistry at the University of Kent at Canterbury. He joined the Weapons Chemistry Branch of AWE in 1980 and studied high explosives compatibility with other weapon components and technologies for tritium management. In 1988 he joined the Personnel Safety Branch of AWE and developed a number of chemical techniques for the assay of toxic and radioactive samples. In 1992 he joined the Process Technology Branch of AWE and specialised in the science of radiological decontamination and assay applied to decommissioning, waste management, environmental remediation and emergency response to radiological incidents. Since 2003 he has continued to specialise in radiological waste assay within the Analytical Sciences Business Unit at AWE.

Farewell to HELEN

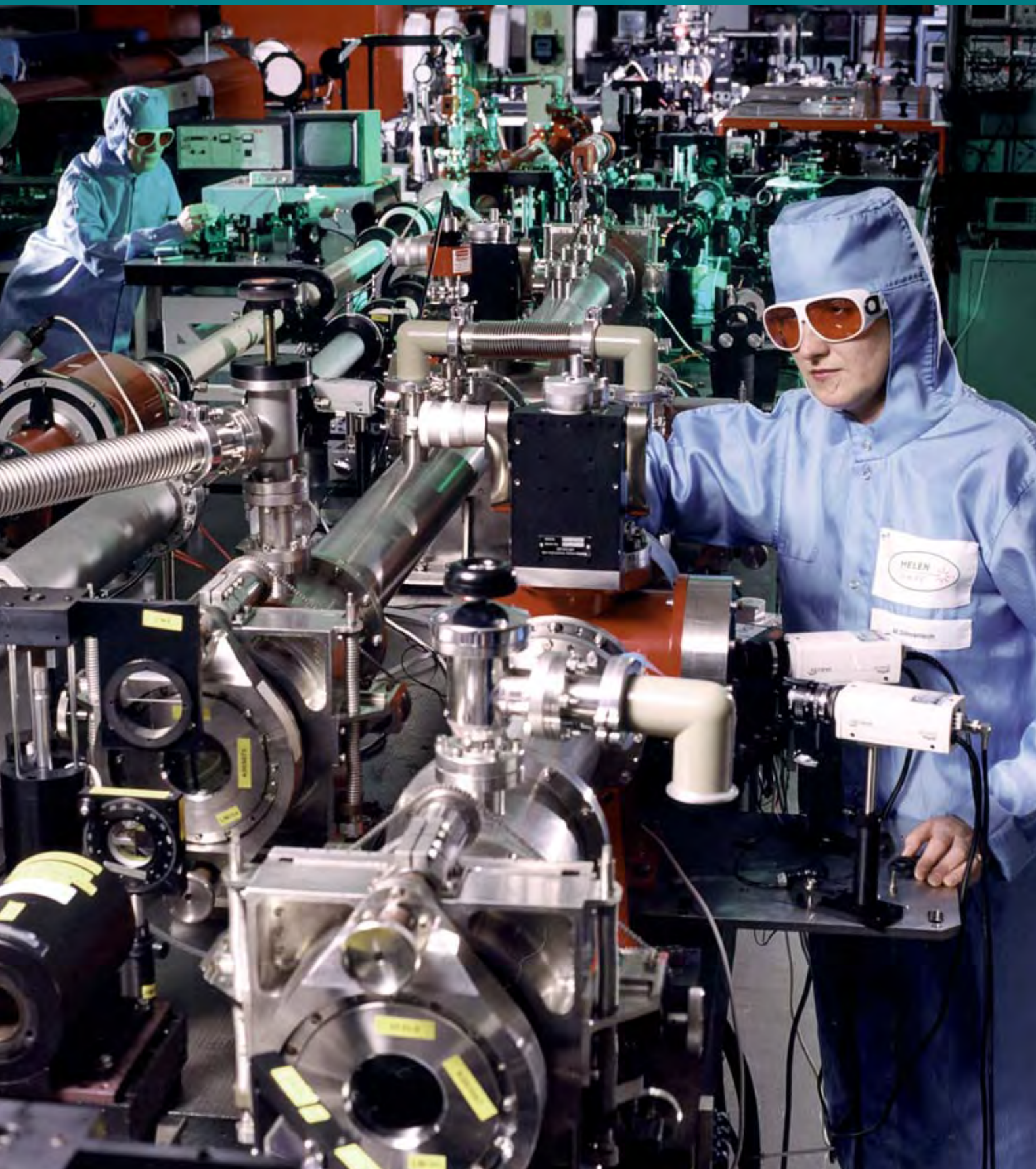

An event marking the closure of HELEN after some thirty years in operation was held on 14th April 2009 at AWE Aldermaston. Over 100 staff from the Plasma and Design Physics departments attended the ceremony, culminating in an emotional farewell to HELEN and an award to recognise the dedication of Roger Clifford (HELEN operations team leader) and the HELEN operations team over the years. Others who attended included special guests Robin Pitman OBE (Associate Director, Institute for Security Science and Technology, Imperial College); Clive Marsh CBE (retired AWE chief scientist); Prof. Mike Dunne (Director, Photon Science Department, Science and Technology Facilities Council); Prof. Steven Rose (Director, Institute of Shock Physics, Imperial College) and Nicola Stanton (Strategic Weapons Project Team, MOD).

HELEN (High Energy Laser Embodying Neodymium) was opened by Her Majesty the Queen on 28th June 1979 and has been a major force in AWE's plasma physics experimental programmes. Her Majesty said:

It is impossible to exaggerate the importance of the work carried out at this Establishment to our security and the preservation of peace. If a deterrent is to deter, and if it is to be credible, the highest standard of science and engineering is required in the design and development of weapons. This high powered laser facility has opened a new chapter in the work of Aldermaston and it will make possible an important research programme for scientists and engineers.

Don Cook (former AWE managing director) opened the ceremony and said:

Since it was opened in 1979, HELEN has shown a strong list of enviable accomplishments. HELEN has enabled the training of many people at AWE, in the plasma physics discipline.

I would like to add that HELEN has also initiated classified work, through the JOWOG collaborations, and unclassified experiments – in plasma physics and secondary science research – underpinning the UK's nuclear deterrence programme.

When we reflect, thirty years from now, I am sure we will say that Orion was built on the shoulders of HELEN and will be uniquely seen as an AWE achievement with international acclaim. We would be without Orion if it were not for HELEN. I would like to show my utmost appreciation and gratitude to all the workers during HELEN's remarkable lifetime.

Tom Bett (group leader operations, Plasma Physics Department) talked about the history of HELEN acknowledging the efforts of hundreds of people over its thirty-year life and reflected that some of the current operating team were not even born when HELEN started. He covered some of the low points as well as the highlights. He noted the irony that when HELEN closed, with the high contrast short pulse addition, the laser was in a unique and world-leading position in accessing high temperature and density conditions in plasma experiments. However, the staff of HELEN are now required for the task of building Orion. The talk finished with the screening of the video made of the countdown for the final shot, which was fired by Roger Clifford. With the last shot fired on 3rd April 2009 the total number of target shots fired, since they first commenced in 1981, was 7940.

Roger Clifford said:

This is a remarkable statistic for such a system. My team and I are immensely proud of our achievement.

HELEN managed to fire 264 target shots in 2006 and then proceeded to smash its

Members of the HELEN team

Roger Clifford receiving his trophy from Tom Bett

The 'Life and Times' of HELEN (1976-2009)...

1976 MOD approves Aldermaston laser facility (ALF1)

1977 Work starts on new AWRE laser facility

1979 Her Majesty Queen Elizabeth II visits AWRE and fires the first HELEN laser shot, marking the official opening of HELEN

1988 First major upgrade – installation of third arm for backlight capability

1994 Control system replaced

1995 Minor upgrade – installation of 208 mm diameter amplifiers on both heating arms

2000 Second major upgrade – Using 208 amplifiers supplied from the US Nova laser facility: HELEN was reconfigured from a single pass to multipass laser system

2001 Minor upgrade – backlighter arm reconfigured into multipass laser system

2002 Minor upgrade – oscillator lab reconfigured for improved operational and safety improvements

2004 Major upgrade – backlighter arm reconfigured from multipass conventional backlighter to an ultra short – pulse Chirped Pulse Amplification (CPA) system. This major step forward brought both the long multipass and short CPA system together to explore new experimental regimes

2007 Record year for target shots fired – 672 in total

2008 453 target shots fired

2009 HELEN closes after nearly 30 years in operation

FIGURE 1

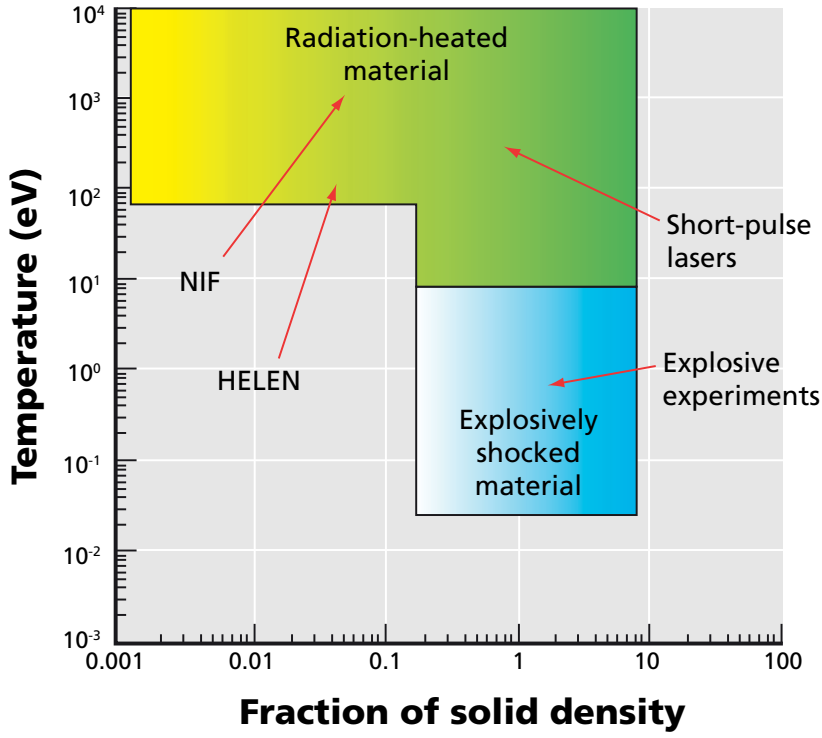

The temperatures and densities reached during the phases of operation of a nuclear warhead (1 eV is approximately 10^4 K).

previous record of target shots in a year (458), made in 1984, by firing 672 successful target shots in 2007. This represents an average of 5 target shots for every day the laser was operational. A similar level of high performance was maintained right up until the facility closed in April 2009. This was only achieved because of the determination, commitment and dedication shown by the exceptional group of people who make up the HELEN operations and support staff.

Roger Clifford was presented with a glass trophy by Tom Bett, in recognition of his outstanding contribution to the operations management of HELEN over the last fifteen years. AWE has made safe the laser while the dismantling process is in progress. Many of the parts are earmarked for loan on systems located in other research organisations in the UK and US, so HELEN will continue to benefit the wider high density plasma physics community.

HELEN Experiments – The Final Chapter

Before it was closed in April this year, the HELEN high power laser[1, 2] was used by AWE scientists to study plasmas relevant to exploding nuclear weapons in controlled laboratory conditions. A plasma is a very high temperature gas in which the atoms separate into ions and electrons; it comprises the majority of the visible matter in the universe in the form of stars and interstellar gas. In 2002 an article in the journal Nature[3] discussed plasma

"For most of its lifetime HELEN operated at ~500 J in 1 ns in each of the 2 beams, providing 100 TW. For comparison the entire power generation capacity of the UK is 50 GW average, 100 GW peak."

physics in the context of nuclear weapons in some detail and stated that to understand the underlying physics of nuclear weapons there is a need to carry out experiments at conditions as close as possible to those in an exploding nuclear weapon.

In order to approach such extremes in the laboratory it is necessary to deliver high power (so energy does not leak away as fast as it is delivered) to a small volume (to ensure high power-density and thus high temperatures). For most of its lifetime HELEN operated at ~500 J in 1 ns in each of the 2 beams, providing 100 TW. For comparison the entire power generation capacity of the UK is 50 GW average, 100 GW peak. Even with these relatively high powers HELEN's long-pulse beams were sufficient to drive experiments to only 100 eV (~1 million degrees Celsius), well short of truly relevant regimes (see Figure 1). To increase the temperature of the plasmas under study it was decided to implement on HELEN a so-called CPA (chirped-pulse amplified) beam as this would increase the available power density on target by a factor of approximately one thousand, albeit for a very short time (1 ps rather than 1 ns).

Calculations suggested that this would produce sample conditions much closer to those of a weapon. This change brought HELEN closer to the forefront of plasma physics research and has been shown in subsequent work to enable much higher temperatures to be accessed, as predicted.

In December 2005 experiments started on HELEN using flat foils irradiated with the 0.5 ps FWHM CPA beam delivering approximately 50 J. Experiments[4-6] showed that although very hot plasmas were undoubtedly being created, they suffered from problems due to pre-pulse, generally inherent in short pulse lasers. This arises because the beam is actually made up of a short pulse part and a much longer lived, lower intensity emission, part of which precedes the short high intensity pulse. The effect of this preceding pulse or pre-pulse is to heat the target and create an unwanted expansion to low density which is very detrimental to the experiments. Moreover, such pre-pulses can often vary randomly making reliable measurements difficult or even impossible.

On HELEN a solution was implemented by converting the light in the CPA beam from infra-red (1.05 μm) to green (0.53 μm) by passing it through an optical component with a non-linear frequency response. This "frequency-doubling crystal" efficiently converts red light to green light at high intensities, but very poorly at low intensities, thus decreasing very significantly the amount of pre-pulse reaching the target.[7] By refining the pulse in this way, while maintaining a high energy in the beam, HELEN became a truly world-leading facility.

Experiments using green light showed a marked difference in the temperatures and densities obtained compared to using infrared. The conditions are inferred from comparison of the measured emission spectra to synthetic spectra generated by mathematical modelling.[4-6] Examples of relatively simple spectra are shown in Figure 2.

FIGURE 2

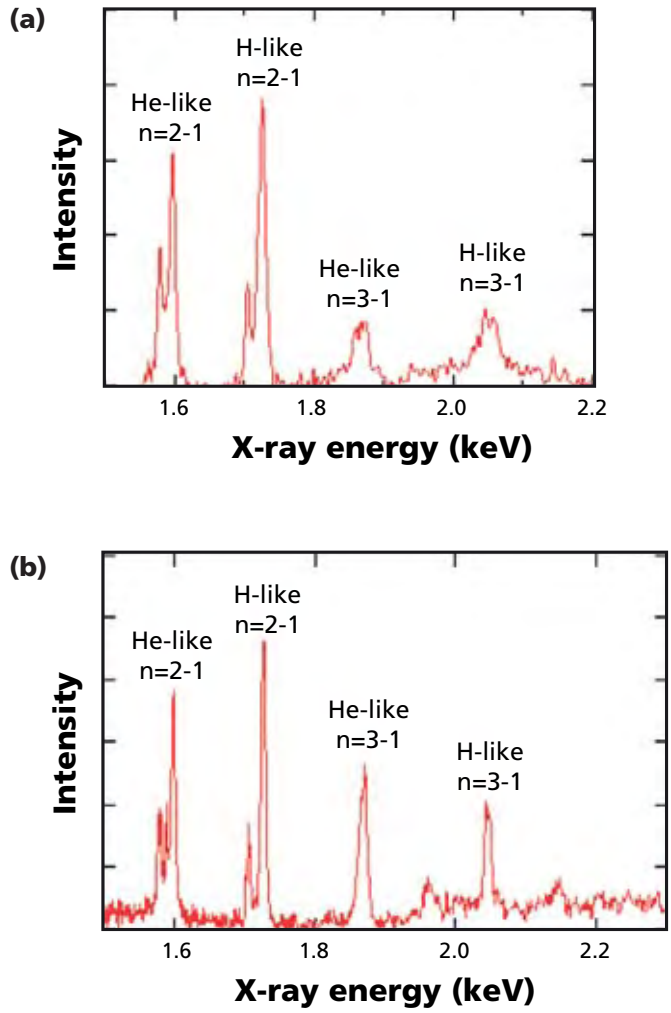

(a) Spectra obtained from an aluminium sample using green light.
(b) Spectra from an aluminium sample with infrared light.

Figure 2(a) shows an emission spectrum from transitions in an aluminium (Al) plasma ionized so that the Al atoms have been stripped of most of their electrons leaving Al ions with the electronic configuration of helium (He) and hydrogen (H). The n in Figure 2 is the principal quantum number of the levels involved in the electron transitions. The ratio of the emission intensities from the different ion species gives the temperature of the plasma and the density can be inferred from the widths of the spectral lines. Note the broader lines in Figure 2(a) where green light was used compared to Figure 2(b) where infrared with a pre-pulse was used. Analysis of these data showed the density was a factor of ten higher in the green light experiments.[4]

In the final weeks of HELEN operations, further experimental progress was made in pushing the experiments to higher density and higher temperatures.[7] One of HELEN's long-pulse beams was shone onto one side of a foil and the short pulse beam

FIGURE 3

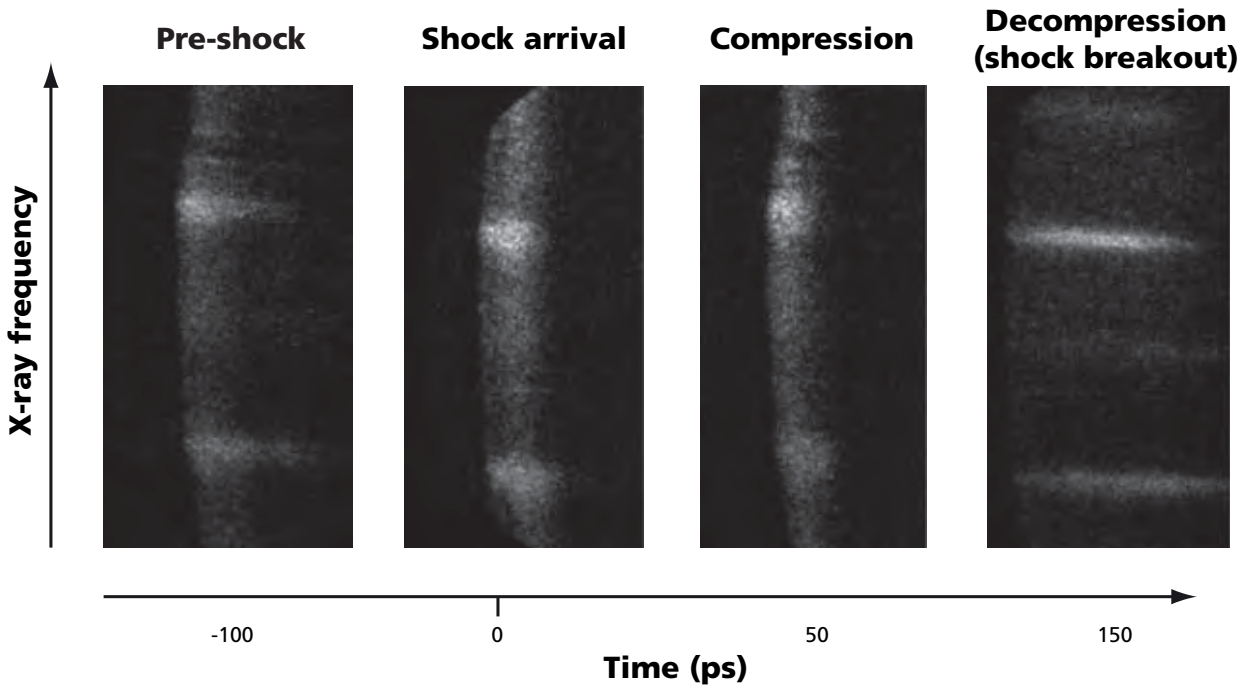

Aluminium buried layer data from the shock compression and short pulse heating experiments, part of the final campaign on HELEN.

onto the other. The foil was made of plastic with a 0.1 μm layer of Al. The long pulse beam sent a shock-wave through the target, compressing the sample, before it was heated by the short pulse beam. Careful synchronization of the long and short pulse beams allowed emission measurements to be made of the material before it expanded following the passage of the shock. The data (Figure 3) showed that the sample reached 650 eV and 3 gcc^{-1}; a higher density than with the CPA alone.

The temperatures of these plasmas are comparable with that near the centre of a star and their densities range from that equivalent of wood to that of solid aluminium metal rather than the tenuous gases more usually associated with high temperature laboratory plasmas.

Figure 3 shows a sequence of results taken at different times in the propagation of the shock wave through the target by varying the timing of the arrival of the long and short pulses. The spectra are those of Al in the frequency range 1.8-2.3 keV covering the transitions from n=1 to n=3 (Figure 2). Before the shock arrives at the Al layer position (the -100 ps frame in Figure 3) the lines are consistent with those seen previously for short pulse only irradiation. As the delay is changed the widths of these lines increases (0 and +50 ps frames), indicating shock compression to higher density and then the lines become narrow as the shock breaks out of the back of the target and the foil begins to decompress (+150 ps frame). There is a similarity between the data in the +150 ps frame and the low density spectra seen in Figure 2b, where the infrared beam with an associated pre-pulse was used.

FIGURE 4

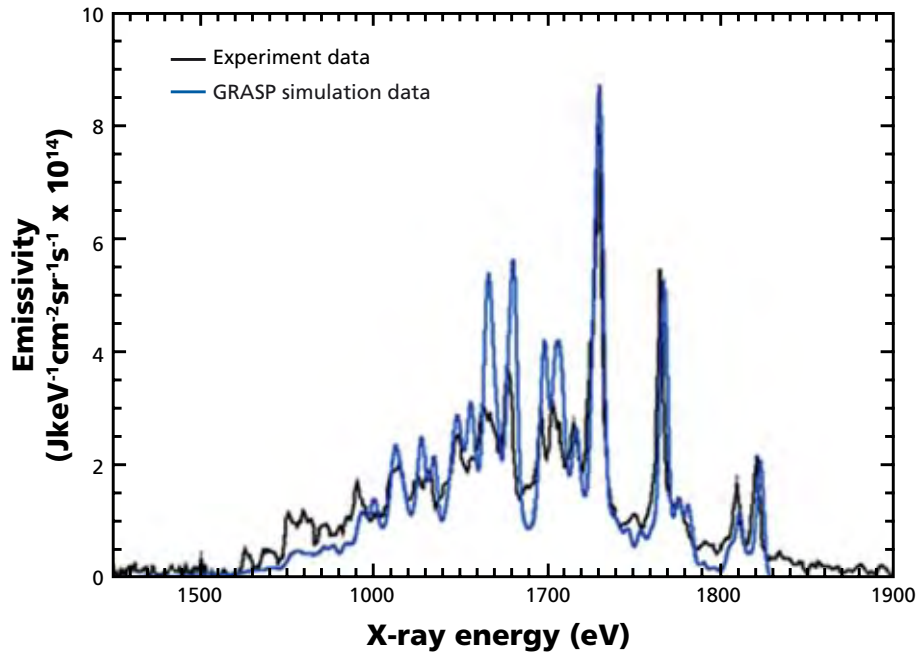

A comparison of experimental data to simulation for the n=3 to n=2 transitions of germanium.

Having established that material can be heated to very high temperature and high densities in a controlled manner, using short pulse lasers and low atomic number elements, experiments were carried out on higher atomic number materials having much more complex spectra. An example of recent experimental data is shown in Figure 4. The spectrum is of n=3 to n=2 transitions in highly ionized germanium (Ge). This is compared to the prediction of a mathematical model developed at AWE.

Comparisons such as the one shown in Figure 4 are used to validate and verify computer models of the behaviour of plasmas under weapon conditions.

Looking forward to Orion

The closure of HELEN does not mean the end of plasma physics experiments at AWE. The Orion project is an ambitious scheme to build a much more powerful laser on site and is planned to commence experiments in 2012. The programme of work on Orion will build on the success of the HELEN CPA experiments to achieve even higher temperatures and densities. The focus for the first experiments will be to study the properties of material at extreme conditions e.g. radiative opacity, equation

FIGURE 5

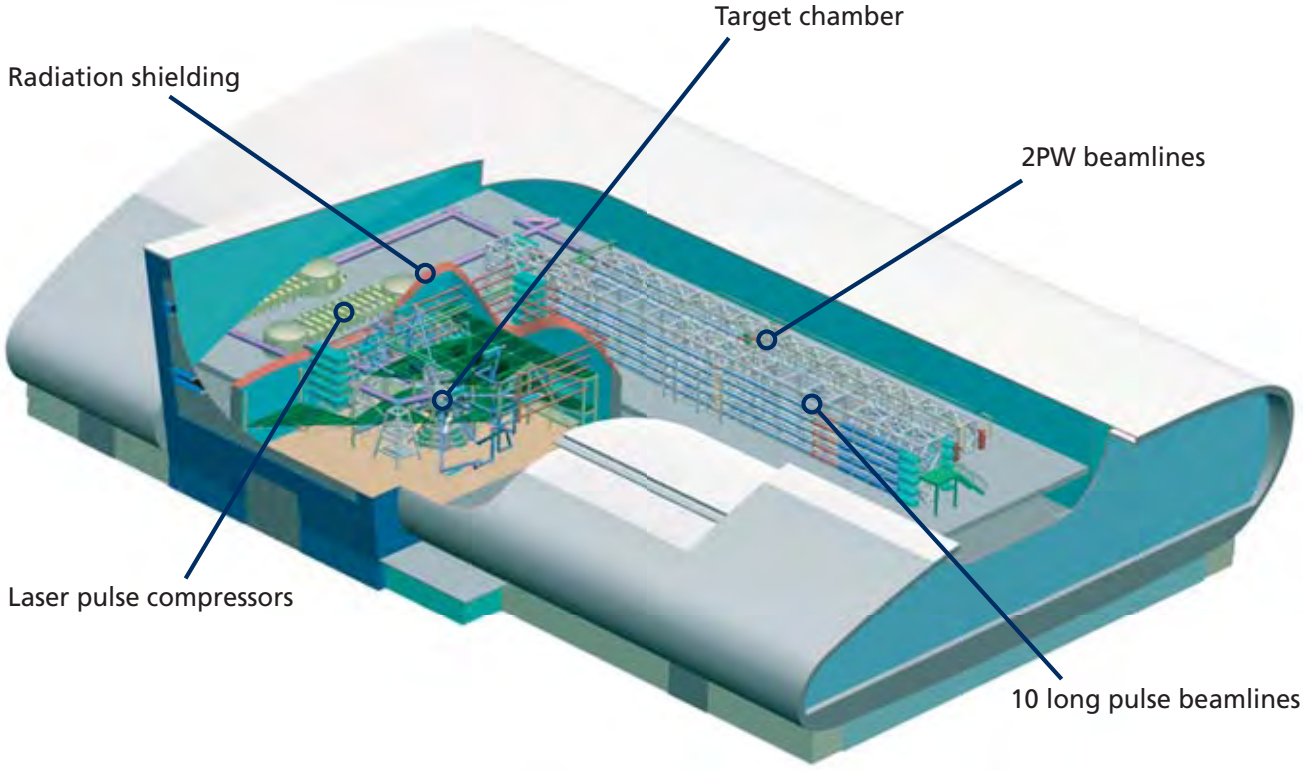

A schematic of Orion cut away to show the component parts of the system.

of state. These experiments will harness the increased energies and powers that Orion will provide. Orion will have ten long-pulse beams, similar to those on HELEN and two CPA beams, similar to that on the Vulcan petawatt laser at the Rutherford Appleton Laboratory. An Orion CPA beam is approximately ten-times more powerful than the CPA beam on HELEN. A cut-away drawing of the Orion laser is shown in Figure 5.

The design of the Orion experiments is being continually updated as more is learnt from the analysis of HELEN experiments. The first Orion experiments are scheduled to start in early 2012 following project completion and work to commission the system.

The Orion laser will be brought up in stages. The first phase is scheduled for completion in December 2010, at which point one long-pulse beam and one short-pulse beam will be available. The remainder of the beams will be completed and commissioned by December 2011, after which full experimental operations will commence. In the interim between HELEN closure and Orion experiments beginning AWE scientists will continue to pursue their research in collaboration with US colleagues at US facilities similar in size to HELEN using some of the parts from the HELEN system including the green conversion optics.

FIGURE 6

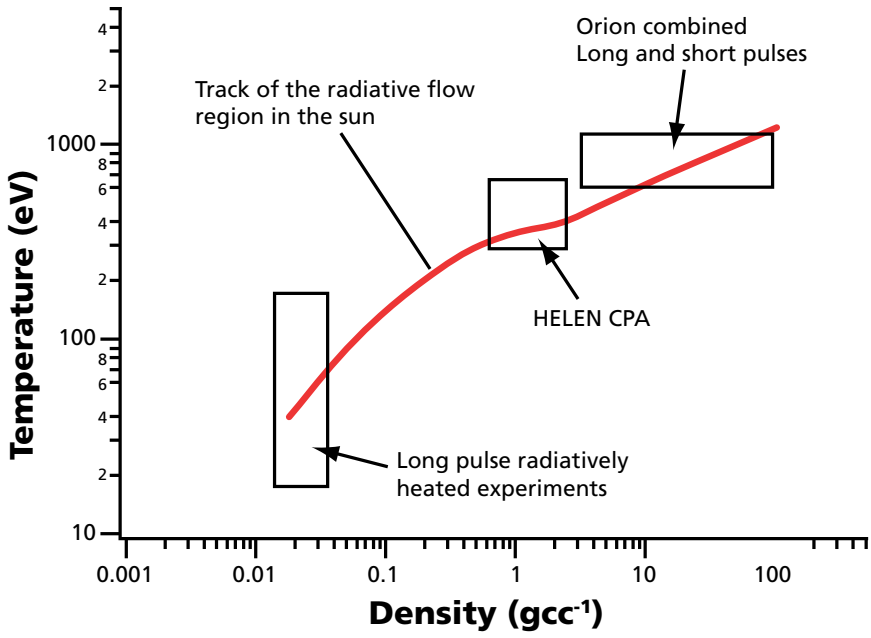

The track of the radiative flow region of the sun in temperature-density space.

Use of Orion by Academic Collaborators

The Orion laser will provide a link between science at AWE and the UK academic community working in the area of plasma physics, astrophysics and high energy density physics. The study of astrophysical phenomena using lasers and other high energy sources, known as laboratory astrophysics, is a growing research field around the world.[8] It will be possible to study issues relevant to solar physics. Figure 6 shows a chart of the temperature-density track of the radiative flow region of the sun.[9] The boxes show the conditions attainable using different methods and facilities. Orion could be used to study plasma over the whole track of conditions plotted including those at the centre of the Sun.

Through the achievements of HELEN, AWE quickly rose to the forefront of plasma physics research. The next generation laser, Orion, will undoubtedly give AWE the oppurtunity to be seen as a global leader in this fundamental area of scientific research..

References

1 M J Norman et al, Applied Optics, 41, 3497 (2002).

2 N. W. Hopps et al, Laser Resonators and Beam Control VIII, Proc. SPIE, 5708, 8 (2005).

3 K. O'Nions, R. Pitman, M. C. Marsh, Nature, 415, 853, (2002).

4 D. J. Hoarty et al, High Energy Density Physics, 3, 115 (2007).

5 D. J. Hoarty et al, pg 114, Plasma Physics Department Annual Report 2006.

6 D. J. Hoarty et al, pg 76, Plasma Physics Department Annual Report 2007.

7 Plasma Physics Department Annual Reports 2005, 2006, 2007.

8 B. A. Remington, Phys. Plasmas 16, 040901 (2009).

9 S. J. Rose, Contemporary Physics, 45, 109 (2004).

If you are involved in an AWE technical event that you would like the editorial team to consider featuring in future editions of Discovery, please contact:

Paul Sagoo
Events & Communications Manager
Tel: 0118 9827 483
Email: Paul.Sagoo@awe.co.uk

AUTHOR PROFILE

Paul Sagoo

Tim Goldsack

David Hoarty

Discovery

Find out more about AWE at our website:

www.awe.co.uk

For further copies of this journal and details of other AWE publications, please write to:

Corporate Communications Office
Building F6.1
AWE Aldermaston
Reading
Berkshire
RG7 4PR

AWE is the trading name of AWE plc
Registered office: Aldermaston Reading Berkshire RG7 4PR
Registered number 3664571

The Science & Technology Journal of AWE • Issue 19 • September 2009